Comparison of the 2010 Chile and 2011 Japan Tsunamis in the Far Field

Jose C. Borrero[1,2] and S. Dougal Greer[1]

Abstract—In this study we analyze water level data from coastal tide gauges and deep-ocean tsunameters to explore the far-field characteristics of two major trans-Pacific tsunamis, the 2010 Chile and the 2011 Japan (Tohoku-oki) events. We focused our attention on data recorded in California (14 stations) and New Zealand (31 stations) as well as on tsunameters situated along the tsunami path and proximal to the study sites. Our analysis considers statistical analyses of the time series to determine arrival times of the tsunami as well as the timing of the largest waves and the highest absolute sea levels. Fourier and wavelet analysis were used to describe the spectral content of the tsunami signal. These characteristics were then compared between the two events to highlight similarities and differences between the signals as a function of the receiving environment and the tsunami source. This study provides a comprehensive analysis of far-field tsunami characteristics in the Pacific Ocean, which has not experienced a major tsunami in nearly 50 years. As such, it systematically describes the tsunami response characteristics of modern maritime infrastructure in New Zealand and California and will be of value for future tsunami hazard assessments in both countries.

Key words: Tsunami, time-series analysis, tide gauge, long waves, spectral analysis, wavelet analysis, ports, harbor resonance, New Zealand, California.

1. Introduction

The tsunamis generated by the 2010 Chile and 2011 Tohoku earthquakes present a unique opportunity to examine the effects of major tsunamis in the far field. These tsunamis complement each other for a number of reasons. First, the events occurred just 1 year apart with source regions located on opposite corners (northwest and southeast) of the Pacific Basin, thus providing an interesting juxtaposition of the distributed effects (Fig. 1). Second, the tsunamis were recorded on a large number of coastal tide gauges and deep-ocean tsunameters. Of interest in this study are the recordings from the relatively dense arrays of tide gauges near New Zealand and California, located at the alternate opposite corners of the Pacific (northeast and southwest) relative to the source regions (northwest and southeast), as well as the recordings of the tsunami wave forms on the Pacific-wide array of Deep-ocean Assessment and Recording of Tsunamis (DART) tsunameters. Third, the Pacific Ocean has not experienced a significant transoceanic tsunami since the 1960 Chile and 1964 Alaska events; thus the 2010 and 2011 tsunamis represent the best source of information on the effects of transoceanic tsunamis on all scales of modern maritime infrastructure. Furthermore, New Zealand and California represent excellent case studies for such an investigation in that both industrial and recreational marine activities are of primary importance to the economies of each region and have expanded dramatically over the past five decades.

2. The 2010 and 2011 Earthquakes and Tsunamis from Chile and Japan

The 27 February 2010 Chile earthquake occurred along South American Subduction Zone (SASZ), which is known to generate great earthquakes and transoceanic tsunamis. This event, the largest from the SASZ in half a century, originated some 230 km north of the source for the largest ever instrumentally recorded earthquake, the great 1960 event. While the 2010 event was a big earthquake, it nucleated relatively deep on the subduction zone, causing the bulk of the energy release (20 m slip at 30 km depth) to

[1] eCoast Ltd., Box 151, Raglan 3225, New Zealand. E-mail: jose@ecoast.co.nz; d.greer@ecoast.co.nz

[2] Department of Civil and Environmental Engineering, University of Southern California, Los Angeles, CA, USA. E-mail: jborrero@usc.edu
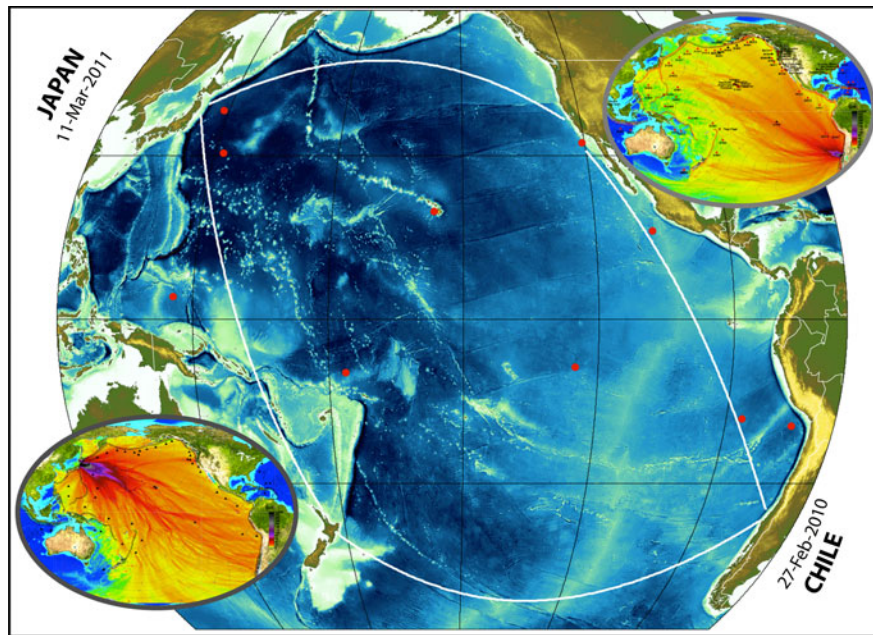
Figure 1
Map of the Pacific Ocean showing the relative locations of the tsunami source regions and the study areas. *Inset* images show the maximum tsunami wave heights for 2010 Chilean (*top right*) and 2011 Japan (*bottom left*) tsunamis as presented by NOAA/NCTR. *Red dots* indicate the locations of the DART tsunameters used in this study

occur at depth and minimizing its tsunami generation potential (DELOUIS *et al.*, 2010; FUJII and SATAKE 2012). Nevertheless the earthquake produced a locally devastating tsunami with runup heights approaching 30 m near Constitución (FRITZ *et al.*, 2011). In contrast, the 11 March 2011 Tohoku, Japan earthquake released nearly twice the energy of the Chilean earthquake, resulting in nearly 30 m of co-seismic slip at 20 km depth and rupture extending to the trench axis (OZAWA *et al.*, 2011) resulting in tsunami runup of over 40 m in the near field (MORI *et al.*, 2011). Numerical modeling results from the US National Oceanic and Atmospheric Administration Center for Tsunami Research (NOAA/NCTR) showing maximum computed tsunami wave heights across the Pacific are reproduced in Fig. 1. Both of these earthquakes generated a significant far-field tsunami observed and recorded throughout the Pacific Basin.

3. Data Sources and Processing

Data used in this study included tide gauge data from New Zealand and California as well as DART tsunameter data. For New Zealand, tide gauge data were obtained from several different sources; however, for the purposes of this study, we refer to two sets of tide gauge data for New Zealand: the "GNS data" and the "NIWA data." The locations of the various tide gauge stations are indicated in Fig. 2.

The GeoNET program of New Zealand's Institute of Geological and Nuclear Science (GNS) collected the GNS data. GNS stations are referred to by a four-letter code such as "AUCT" for Auckland. We downloaded the 1-Hz "LTT" dataset which is provided with the tide signal removed from GNS's publicly accessible FTP server. We then processed the 1-Hz data by wavelet denoising, using a universal threshold and a symlet wavelet with scaling factor of 8, as well as high-pass filtering to remove residual low-frequency oscillations. The processed 1-Hz data were used for assessing arrival times and wave heights and for the Fourier analysis, while 1 min-averaged data were used for the wavelet analysis to be compatible with the other datasets.

The "NIWA" gauges represent data from a network of gauges coordinated by New Zealand's National Institute of Water and Atmospheric
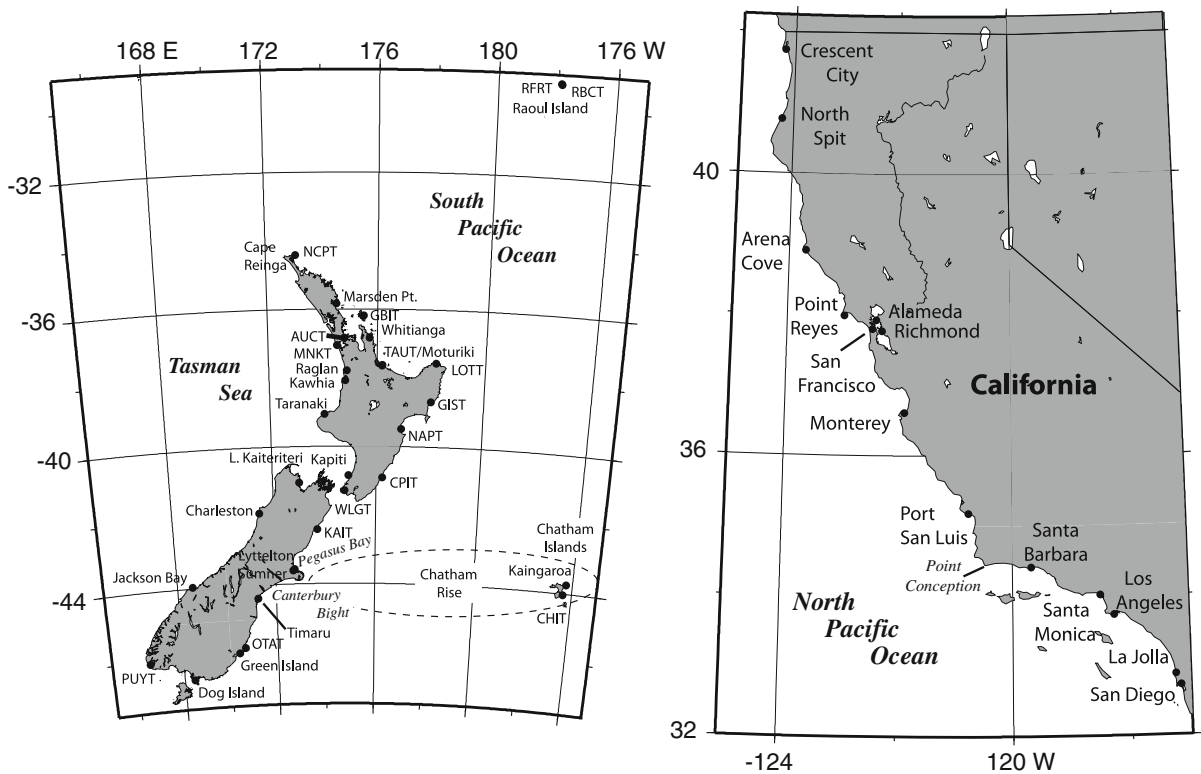
Figure 2
Maps of New Zealand and California showing the locations of the tide gauge stations used in this study

Research (NIWA). Gauges in this set include water level records from gauges maintained by: (a) port companies at Tauranga, Taranaki (New Plymouth), Lyttelton (Christchurch), and Timaru; and (b) local government agencies (Northland and Waikato Regional Councils and Tasman District Council); and (c) the National Tide Center–Bureau of Meteorology, Australia (Jackson Bay Gauge). NIWA gauges are referred to by full location names such as "Sumner Head." Data were provided at 1 min sampling after detiding and band-pass filtering to remove high-frequency noise and residual low-frequency tidal signals (ROB BELL, pers. comm.).

For the California gauges, we obtained data from instruments maintained by the National Oceanic and Atmospheric Administration (NOAA). Data were downloaded from publicly accessible NOAA servers as detided 1 min data. This was subsequently wavelet denoised, using a symlet wavelet with scaling factor of 2, and high-pass filtered.

Deep-water tsunami data were obtained from NOAA's array of DART tsunameters deployed throughout the Pacific Ocean. The DART data used in this study were postprocessed by staff at NOAA's Pacific Marine Environmental Laboratory (PMEL) using a Butterworth-type high-pass filter with a 2–4 h cutoff period depending on the character of the tsunami signal. This method is appropriate in this case as the time series is long enough that tail effects do not interfere with the main signal. This process is performed manually with the different levels of filtering compared before deciding on a final dataset (YONG WEI, pers. comm.). We then further processed the data through manual despiking where necessary. DART data provided at 15 s sampling was used for the Fourier analysis and downsampled to 1 min for wavelet analysis.

Our analysis of these time series presented here includes: (1) statistical description of each time series, (2) FFT analysis of the sea level data and (3)

wavelet analysis of the sea level in the days after the arrival of the tsunami to understand the development of different frequency components through the duration of the tsunami effects.

3.1. Time-Series Analysis

The residual water level time series for both tsunamis in California and New Zealand are plotted in Figs. 3a, b, 4a, b, and 5a, b. The residual data were denoised using wavelet denoising with a universal threshold. High-pass filtering was carried out using discrete wavelet filtering. The time series were analyzed for tsunami arrival times, maximum tsunami wave amplitudes, maximum peak-to-trough (P2T) tsunami heights, and associated times for each quantity (Tables 1, 2, 3). Arrival times were determined through visual inspection of the time series. Maximum tsunami amplitudes, associated troughs, and maximum P2T values were determined through a quasiautomated process over the first 60 h of available data (approximately 40–50 h after tsunami arrival). Maximum amplitudes were determined by analyzing the time series for inflection points after each zero-crossing of the water level trace. The data values at each inflection point were then compared to determine maximum values. For the trough associated with this maximum amplitude, we selected the lowest value of the inflection point occurring either immediately before or immediately after the chosen maximum amplitude. The sum of these two quantities is designated the "tsunami height at maximum amplitude." In some cases this value is the same as the maximum peak-to-trough value determined by computing the difference between inflection points on either side of a zero-crossing. The maximum sea level (SL) is the maximum positive value of the water level time series above the computed mean over the entire data record and includes the effect of the tide.
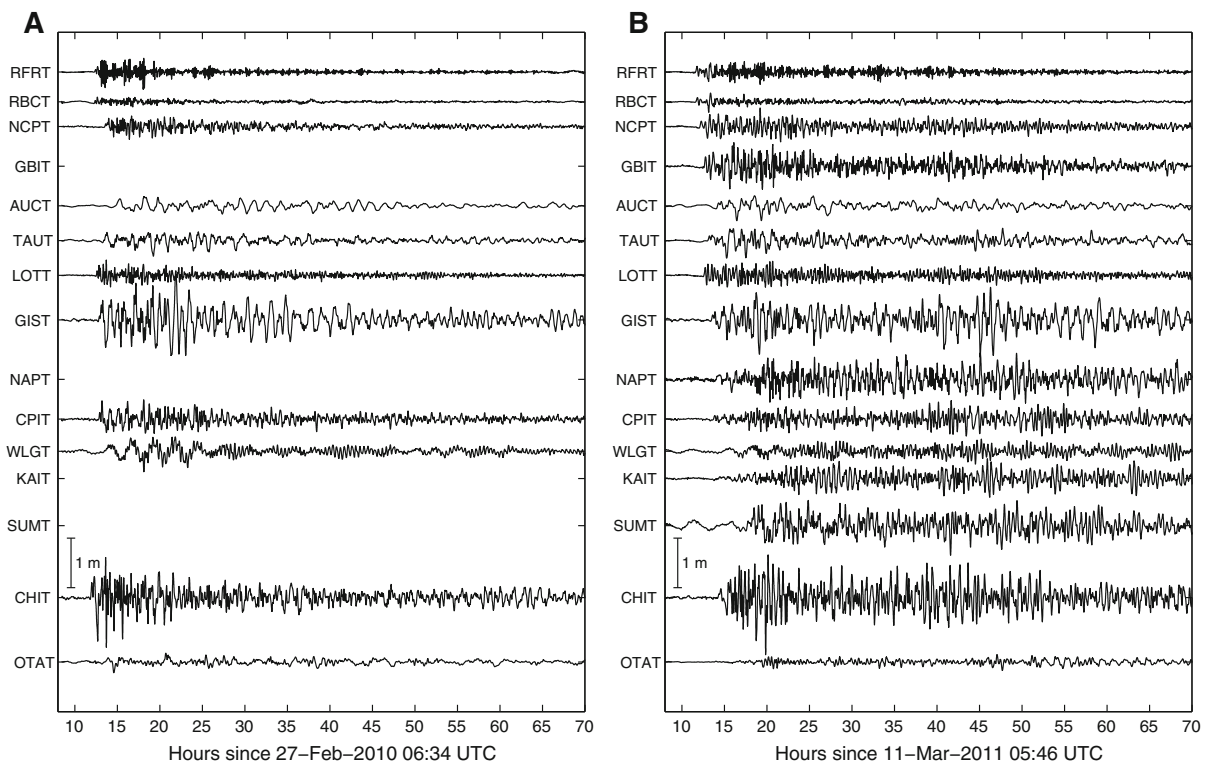

Figure 3
Residual tsunami water levels from the GNS gauges in New Zealand: Chile tsunami (*left*) and Japan tsunami (*right*)
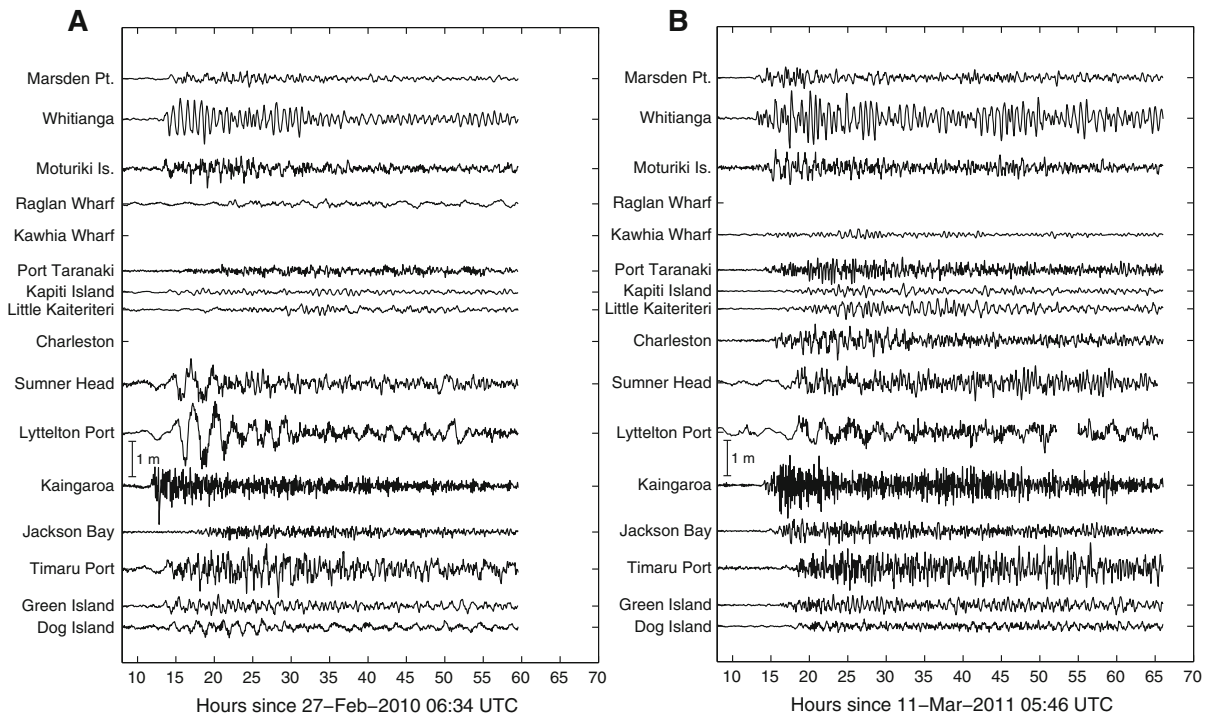
Figure 4
Residual tsunami water levels from the NIWA gauges in New Zealand: Chile tsunami (*left*) and Japan tsunami (*right*)
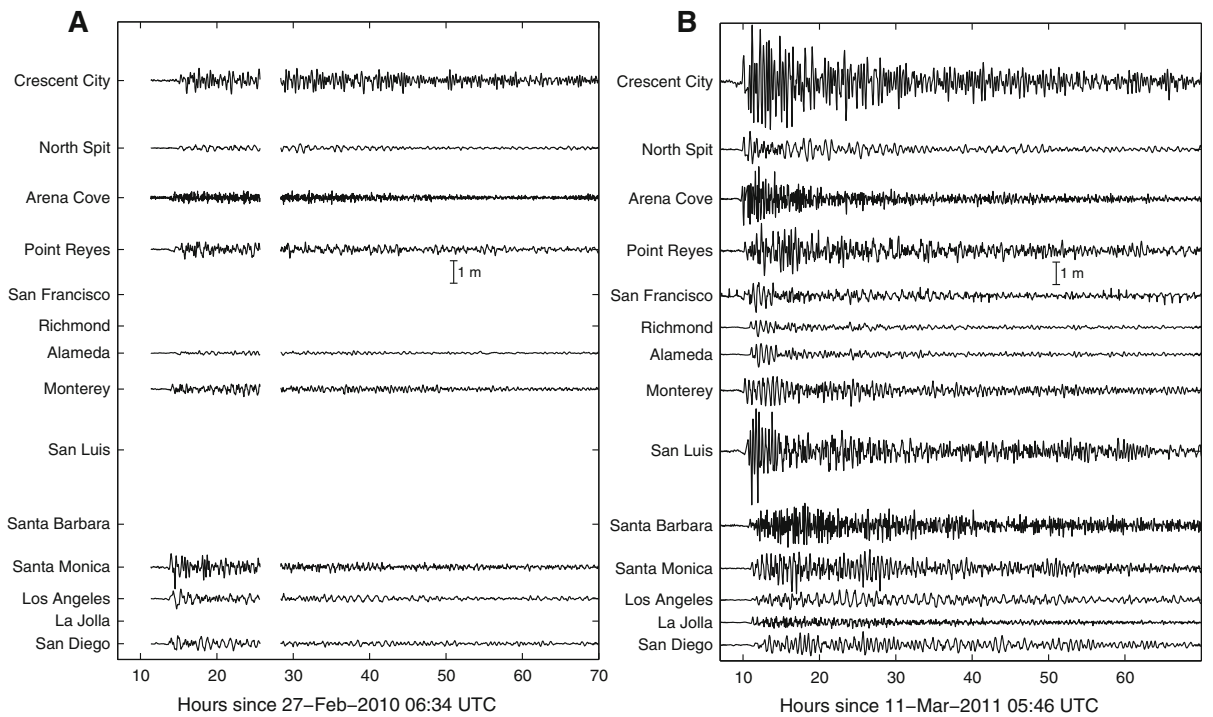

Figure 5
Residual tsunami water levels from the NOAA gauges in California: Chile tsunami (*left*) and Japan tsunami (*right*)

Table 1

Summary statistics for the Japan and Chile tsunamis on the GNS tide gauges in New Zealand

Station	Arrival time	Max. amp.	Assoc. trough	Height	Hours after arrival	Max. P2T	Hours after arrival	Max. SL	Hours after arrival
GNS–Chile									
RFRT	12.34	0.28	−0.35	0.62	5.77	0.62	5.77	0.69	23.90
RBCT	12.26	0.09	−0.04	0.14	0.38	0.18	4.07	0.68	36.92
NCPT	13.46	0.21	−0.26	0.47	3.21	0.47	3.21	1.22	23.70
GBIT	N/A	N/A	N/A	N/A	N/A	N/A	N/A	N/A	N/A
AUCT	14.58	0.19	−0.11	0.29	3.55	0.31	14.87	1.61	22.60
TAUT	13.28	0.17	−0.21	0.38	11.24	0.48	5.37	0.97	24.17
LOTT	12.50	0.31	−0.19	0.49	1.20	0.49	1.20	1.03	23.46
GIST	12.74	0.99	−0.71	1.7	9.13	1.7	9.13	1.59	9.13
NAPT	N/A	N/A	N/A	N/A	N/A	N/A	N/A	N/A	N/A
CPIT	12.81	0.39	−0.29	0.67	5.29	0.67	5.29	1	47.19
WLGT	13.63	0.29	−0.21	0.5	8.18	0.5	8.18	0.75	20.20
KAIT	N/A	N/A	N/A	N/A	N/A	N/A	N/A	N/A	N/A
SUMT	N/A	N/A	N/A	N/A	N/A	N/A	N/A	N/A	N/A
CHIT	11.90	0.81	−1	1.81	1.72	1.81	1.72	1	9.66
OTAT	13.59	0.18	−0.09	0.27	7.11	0.3	1.62	1.28	19.44
GNS–Japan									
RFRT	11.52	0.21	−0.13	0.34	5.82	0.42	7.75	0.72	5.82
RBCT	11.60	0.18	−0.21	0.39	1.77	0.39	1.77	0.62	5.68
NCPT	12.06	0.38	−0.21	0.58	7.14	0.58	7.14	1.01	7.14
GBIT	12.61	0.48	−0.45	0.93	3.50	0.93	3.50	1.02	5.60
AUCT	14.01	0.2	−0.08	0.28	4.54	0.44	2.99	1.18	4.54
TAUT	13.00	0.25	−0.11	0.36	34.72	0.59	3.05	0.85	5.57
LOTT	12.52	0.29	−0.23	0.51	8.15	0.51	8.15	0.84	4.54
GIST	13.44	0.66	−0.72	1.38	32.86	1.38	32.86	0.95	5.29
NAPT	13.99	0.53	−0.34	0.87	31.11	0.94	35.37	0.86	16.53
CPIT	13.69	0.38	−0.31	0.69	27.98	0.69	27.98	0.84	27.98
WLGT	16.31	0.25	−0.15	0.39	28.91	0.48	28.40	0.68	37.10
KAIT	15.96	0.4	−0.38	0.78	29.97	0.78	29.97	0.89	12.54
SUMT	16.86	0.51	−0.14	0.65	7.99	0.91	31.07	1.16	11.72
CHIT	14.16	0.86	−1.15	2.01	5.97	2.01	5.97	1.05	14.64
OTAT	16.19	0.15	−0.04	0.18	30.88	0.24	4.36	0.7	36.46

Arrival time is in hours after the earthquake and water levels are in meters

3.2. Spectral (FFT and Wavelet) Analysis

The frequency content of the resulting time series was quantified through both Fast Fourier Transform (FFT) and wavelet analysis. The FFT analysis provides an indication of the dominant frequencies present in each time series over the course of the tsunami. Due to the nonperiodic nature of the signal, windowing was incorporated to minimize spectral leakage. This was carried out using a Hann window with 50 % overlap to provide a degree of spectral smoothing as described in EMERY and THOMSON (2003) and applied by RABINOVICH and THOMSON (2007) to data recorded on tide gauges throughout the Indian Ocean following the 2004 Boxing Day tsunami. In addition, because the frequency content of the sea level record at each location changes with time and because the FFT only provides a snapshot of frequencies present in the signal, we use just a subset of each record starting at the time of tsunami arrival as described below.

For the 1 s GNS time series, 81,920 samples (~22.8 h) of the tsunami signal was used for FFT analysis, providing three windows of 32,768 records (~9.1 h). For the 1 min NIWA and NOAA-California gauges, 1,280 samples (21.3 h) were used with four 512-sample (8.5 h) windows. Because the effects

Table 2

Summary statistics for the Japan and Chile tsunamis on the NIWA tide gauges in New Zealand

Station	Arrival time	Max. amp.	Assoc. trough	Height	Hours after arrival	Max. P2T	Hours after arrival	Max. SL	Hours after arrival
NIWA–Chile									
Marsden Pt.	14.00	0.22	−0.24	0.46	10.27	0.46	10.27	1.34	23.35
Whitianga	13.34	0.59	−0.45	1.04	2.23	1.23	4.99	1.18	23.56
Moturiki Is.	13.20	0.35	−0.42	0.77	10.30	0.77	10.30	1.29	10.30
Raglan Wharf	21.66	0.15	−0.11	0.26	12.87	0.26	12.87	1.88	18.47
Kawhia Wharf	N/A	N/A	N/A	N/A	N/A	N/A	N/A	N/A	N/A
Port Taranaki	16.14	0.19	−0.06	0.25	4.88	0.38	16.43	2	23.14
Kapiti Island	13.67	0.11	−0.05	0.16	4.86	0.21	23.45	1.16	26.28
Little Kaiteriteri	18.53	0.17	−0.1	0.27	12.80	0.3	16.27	2.17	21.20
Charleston	N/A	N/A	N/A	N/A	N/A	N/A	N/A	N/A	N/A
Sumner Head	11.69	0.72	−0.48	1.2	5.28	1.2	5.28	1.44	22.88
Lyttelton Port	11.78	0.91	−0.77	1.68	8.30	1.86	5.42	1.74	8.30
Kaingaroa	11.60	0.54	−0.33	0.88	0.67	1.61	1.13	0.94	10.13
Jackson Bay	17.60	0.2	−0.19	0.38	10.13	0.4	20.33	1.66	23.33
Timaru Port	13.54	0.72	−0.53	1.24	13.26	1.29	10.91	1.55	18.19
Green Island	12.95	0.33	−0.19	0.52	7.57	0.52	7.57	1.27	19.40
Dog Island	14.08	0.25	−0.22	0.48	12.09	0.51	7.07	1.64	29.47
NIWA–Japan									
Marsden Pt.	12.89	0.31	−0.28	−0.59	4.03	0.59	4.03	1.05	5.51
Whitianga	13.04	0.78	−0.85	−1.63	4.64	1.63	4.64	1.28	4.64
Moturiki Is.	13.03	0.52	−0.38	−0.9	2.57	0.92	4.04	1.17	5.52
Raglan Wharf	N/A	N/A	N/A	N/A	N/A	N/A	N/A	N/A	N/A
Kawhia Wharf	14.04	0.16	−0.11	−0.27	12.31	0.27	12.31	0.92	7.08
Port Taranaki	13.94	0.36	−0.21	−0.57	18.18	0.73	9.13	1.12	7.14
Kapiti Island	15.59	0.22	−0.17	−0.39	16.68	0.39	16.68	0.62	16.68
Little Kaiteriteri	16.03	0.3	−0.15	−0.45	21.79	0.51	8.25	1.11	4.67
Charleston	14.83	0.47	−0.39	−0.85	5.92	0.88	8.30	1.1	5.94
Sumner Head	16.94	0.49	−0.17	−0.66	32.48	0.92	30.99	1.18	11.64
Lyttelton Port	17.24	0.47	−0.22	−0.69	1.43	0.79	33.18	1.11	11.51
Kaingaroa	13.81	0.84	−0.65	−1.5	3.66	1.5	3.66	1.21	2.42
Jackson Bay	14.43	0.35	−0.33	−0.68	4.65	0.69	3.57	0.8	7.39
Timaru Port	16.44	0.72	−0.43	−1.14	40.16	1.24	34.16	1.13	37.18
Green Island	16.13	0.3	−0.16	−0.46	6.99	0.52	9.52	0.78	36.42
Dog Island	18.13	0.21	−0.14	−0.34	9.00	0.34	9.00	0.8	31.70

Arrival time is in hours after the earthquake and water levels are in meters

of the tsunami on recorded sea level are apparent at the deep-water DART sites for less time than at coastal locations, a shorter, 2,048 sample record (8.5 h at 15 s) was used for the FFT using three 1,024-sample windows. To provide increased resolution at lower frequencies, for the NIWA, DART, and NOAA datasets each window was padded with zeros to eight times the window length. For the 1 s GNS data, padding was reduced to four times the window length.

Wavelet analysis follows the evolution of the frequency content of the sea level records over the duration of the tsunami events. It performs a similar function as short-term Fourier transform (STFT) in that it can be used to analyze time series that contain nonstationary power at many different frequencies, as is the case here where dominant observed frequencies are dependent on the interaction between the incoming tsunami and the resonant frequencies of the receiving environment. The method used here follows that described by TORRENCE and COMPO (1998). Wavelet analysis was carried out using a Morlet wavelet, as it is complex and therefore useful for identifying changes in frequency components over time. It is also a wavelet which has moderate width in

Table 3

Summary statistics for the Japan and Chile tsunamis on the NOAA tide gauges in California

Station	Arrival time	Max. amp.	Assoc. trough	Height	Hours after arrival	Max. P2T	Hours after arrival	Max. SL	Hours after arrival
CA–Chile									
Crescent City	15.00	0.54	−0.33	0.87	2.67	1.1	15.48	1.61	21.47
North Spit	15.02	0.19	−0.23	0.42	15.91	0.42	15.91	1.28	21.65
Arena Cove	14.31	0.32	−0.27	0.58	17.79	0.6	20.77	1.23	20.77
Point Reyes	14.40	0.33	−0.36	0.69	4.13	0.71	1.00	1.19	21.27
San Francisco	N/A	N/A	N/A	N/A	N/A	N/A	N/A	N/A	N/A
Richmond	N/A	N/A	N/A	N/A	N/A	N/A	N/A	N/A	N/A
Alameda	14.75	0.1	−0.09	0.19	2.97	0.2	23.17	1.15	21.75
Monterey	14.01	0.23	−0.2	0.43	2.02	0.56	9.86	1.02	21.07
Port San Luis	N/A	N/A	N/A	N/A	N/A	N/A	N/A	N/A	N/A
Santa Barbara	N/A	N/A	N/A	N/A	N/A	N/A	N/A	N/A	N/A
Santa Monica	13.85	0.6	−0.97	1.57	0.17	1.57	0.17	1.15	20.63
Los Angeles	13.79	0.42	−0.46	0.88	1.49	0.88	1.49	1.25	20.29
La Jolla	N/A	N/A	N/A	N/A	N/A	N/A	N/A	N/A	N/A
San Diego	13.68	0.36	−0.28	0.64	1.20	0.64	4.27	1.26	20.19
CA–Japan									
Crescent City	9.82	2.53	−1.8	4.33	1.36	4.33	1.36	1.76	9.23
North Spit	9.88	0.8	−0.64	1.44	1.04	1.44	1.04	1.07	19.95
Arena Cove	9.77	1.44	−1.01	2.45	2.30	2.45	2.30	1.11	19.63
Point Reyes	10.10	1.22	−0.59	1.8	2.30	2.07	6.77	1.23	20.27
San Francisco	10.06	0.59	−0.73	1.33	2.01	1.33	2.01	0.91	20.76
Richmond	10.89	0.31	−0.41	0.73	1.39	0.73	1.39	0.76	19.61
Alameda	10.96	0.48	−0.56	1.04	1.41	1.04	1.41	0.86	19.61
Monterey	10.07	0.62	−0.68	1.3	3.85	1.3	3.85	0.94	18.58
Port San Luis	10.24	1.89	−2.28	4.17	1.46	4.17	1.46	1.38	3.56
Santa Barbara	10.73	1.0	−0.84	1.84	7.37	1.84	7.37	1.27	18.40
Santa Monica	10.98	0.83	−0.59	1.43	15.62	1.8	5.69	1.38	15.62
Los Angeles	11.04	0.46	−0.31	0.77	12.49	0.77	12.49	0.96	16.44
La Jolla	11.09	0.27	−0.17	0.44	6.98	0.46	2.59	0.73	16.18
San Diego	11.44	0.6	−0.44	1.04	14.29	1.04	14.29	1.12	14.29

Arrival time is in hours after the earthquake and water levels are in meters

both the time and frequency domain, allowing for reasonable resolution in both dimensions (TORRENCE and COMPO, 1998).

4. Discussion

4.1. Wave Heights and Arrival Times

The summary statistics for the tsunami wave heights and arrival times are listed in Tables 1, 2, 3. Time-series plots for all of the stations analyzed are presented in Figs. 3, 4, 5. For the Chilean event, tsunami waves reached the east coast of New Zealand and southern California at around the same time,

approximately 13 h after the earthquake. In the Japan event, waves reached northern California after 9 h, southern California in 10 h, and New Zealand in 12–14 h. Starting with New Zealand, we see that during the Japan tsunami, there is a clear demarcation on the GNS stations between the timing of the maximum amplitude and maximum P2T values for stations located in the northern part of the North Island (NCPT, GBIT, AUCT, and LOTT) and those located on the east coast of the North and South Islands (GIST, NAPT, CPIT, WLGT, KAIT, SUMT, and OTAT). Those in the north experienced the maximum tsunami heights between 3 and 8 h after tsunami arrival, whereas this occurred approximately 30 h after arrival for most of the eastern and southern

stations. The exception to this is the TAUT gauge, which experienced the highest amplitude at 34.7 h after arrival. However, while this is the maximum, this amplitude is within a few centimeters of amplitudes recorded much earlier in the time series. This general pattern is also evident for the maximum overall sea levels. For stations located on Raoul or the Chatham Islands, the maxima occurred relatively early in the tsunami signal ($\sim$2–6 h), with the exception of CHIT ($\sim$14.6 h). We also note that for many of the stations, the tsunami height at maximum amplitude occurs in the same wave cycle as the maximum P2T tsunami height. In some cases, particularly in the north of New Zealand, this also coincided with the overall maximum sea level. One notable exception is GIST, where the maximum amplitude and maximum P2T occurred nearly 33 h after tsunami arrival while the maximum overall sea level occurred after just 5.3 h.

During the 2010 Chilean tsunami in New Zealand, these patterns are not as clear. There is no apparent regional demarcation in the timing of the maximum wave heights or water levels. For all stations, the maximum amplitude and maximum P2T values occur within 10 h of the tsunami arrival. Maximum overall water levels occur later, between 10 and 37 h after tsunami arrival. It is also notable that, for the Chilean tsunami, the maximum tsunami amplitude, maximum P2T, and overall water level are all greater than for the Japan event at stations located on the east coast of the North and South Islands (GIST, Sumner, Lyttelton, and Timaru). The opposite is true for stations in the north and east of the North Island such as NCPT, TAUT, and Moturiki and on the west coast (Taranaki, Kapiti, Little Kaiteriteri, and Jackson Bay). Whitianga and stations in the Chatham Islands (Kaingaroa and CHIT) experienced much larger waves during the Japan tsunami as compared with the Chilean event. LOTT, which is located on New Zealand's East Cape, recorded nearly equivalent wave heights for both events, as did the stations in the far south (Green Is. and Dog Is.).

In California, data from the Tohoku tsunami (Table 3a) indicate some demarcation in the timing of the maximum amplitudes between the northern and central California stations relative to those in southern California. At the northern stations, the

maximum amplitudes occurred between 1 and 4 h after arrival, whereas in the south (Santa Barbara to San Diego) the maximum amplitude occurred 7–16 h after arrival. This distinction is also true for the maximum P2T values, as the maximum amplitude wave coincided with the maximum P2T wave at all of the northern stations except for Point Reyes. Three of the five southern stations also had the maximum amplitude on the same cycle as the maximum P2T. Santa Monica and La Jolla experienced the maximum P2T wave height prior to the wave cycle with the maximum amplitude. Indeed, Santa Monica's maximum P2T wave height occurred 5.6 h after first arrival, nearly 10 h before the cycle with the maximum positive amplitude. Maximum sea levels generally occurred 14–20 h after tsunami arrival with exceptions at San Luis (3.5 h post-arrival) and Crescent City (9.2 h post-arrival).

During the Chilean tsunami, the southern stations (SD, LA, and SM) all experienced the maximum amplitude and P2T on the same wave cycle, occurring shortly after arrival (0.17–1.2 h). Northern stations also generally saw the maximum amplitude within a few (2–4) hours after wave arrival, with the exceptions of North Spit and Arena Cove at 15.9 and 17.8 h, respectively. Maximum P2T wave heights during the Chilean tsunami in Northern California generally occurred later than the maximum amplitude, with the exception of Point Reyes where it occurred 3 h earlier.

The rough generalizations that can be drawn from this information are summarized in the following points.

For the Tohoku tsunami in New Zealand:

- Stations in the north experienced the largest waves, both maximum positive amplitude and maximum P2T, within 10 h of first arrival.
- Stations on the east coast of the North and South Islands experienced these maxima much later, on the order of 30 h after first arrival. The notable exception is Lyttelton, which saw the maximum positive amplitude just 0.3 h after tsunami arrival.

For the Tohoku tsunami in California:

- Maximum amplitudes and P2T wave heights occurred shortly after first arrival on northern

gauges (generally 1–4 h) and later on southern gauges (7–15 h) with a few exceptions.

For the Chile tsunami in New Zealand:

- Maximum amplitude and P2T wave heights generally occurred within the first 10 h after wave arrival at sites located on northern and eastern coasts. These maxima were generally later on west coast gauges.

For the Chile tsunami in California:

- Southern California stations saw the maximum amplitudes and P2T wave heights shortly after first arrival (0.2–1.5 h).
- At most northern California stations these maxima occurred later, 15–20 h after arrival with some exceptions.

4.2. Spectral Analysis

The spectral analysis of the tsunami signals consisted of FFT and wavelet analysis. The purpose of this analysis is to determine the dominant response frequencies of the various receiving environments. In some cases, this is an open coast site such as Point Arena or Port San Luis in California or KAIT (Kaikoura) and NCPT (North Cape) in New Zealand, where we would expect to see a relatively "clean" tsunami signal free from basin effects. Other sites such as North Spit (inside Humboldt Bay, California), Los Angeles and San Diego in California, and Tauranga (TAUT) or Auckland (AUCT) in New Zealand are situated inside large embayments or natural and manmade harbors. Still other sites, such as Crescent City in California or Whitianga, Gisborne, and Lyttelton in New Zealand, are known to resonate and amplify long waves and have previously experienced the damaging effects of tsunami waves. We performed an FFT analysis on each of the water level time series and plotted them for both events (Fig. 6a–c) at each station to facilitate comparison between the two tsunamis. Spectral peaks were identified by visual inspection and are collated in Table 4a–d in order of decreasing energy. In some cases, a clear peak could not be clearly defined, thus a range of periods is indicated.

4.2.1 Review of Spectral Analyses for Tsunami in New Zealand and California

A significant transoceanic tsunami has not affected the Pacific Ocean since the 1960 and 1964 events. Several studies have described the far-field tsunami characteristics at locations in both California and New Zealand. For example, MILLER *et al.* (1962) reported on the spectral characteristics of the 1960 tsunami at La Jolla. Their analysis compared the tsunami signal versus background noise and showed very clearly the persistence of the tsunami, particularly at lower frequencies, which stayed above background levels for more than 5 days.

RAICHLEN (1970) described the spectral characteristics of tide gauge records from the 1960 Chile and 1964 Alaska tsunamis at several locations on the North American west coast and two Pacific Islands. For the 1964 Alaska event, he found that the spectral response at three California sites (Santa Monica, Los Angeles, and La Jolla) were roughly similar with spectral peaks at periods of 33–38 min and 100–150 min. He also showed that, at Los Angeles, these peaks were evident during the 1960 Chile tsunami. Furthermore, he noted that a spectral peak centered at roughly 2 h was also evident on recordings of the 1960 and 1964 tsunamis at Pago Pago and Midway Island. Besides the low-frequency component ubiquitous to these sites for both events, RAICHLEN (1970) noted that the higher-frequency components at each site were most likely dependent on the geometric specifics of that particular location.

Several examples of spectral analysis for sites in New Zealand are also available. HEATH (1976) analyzed the response of several New Zealand harbors to the 1960 Chile tsunami, and among other observations, noted a resonance of 160 min at Lyttelton and Wellington. He also presented additional data for the 1964 tsunami in Lyttelton, also showing a spectral peak at 160 min, however that signal also included a much stronger peak at 96 min. The response of Wellington Harbor to the 1960 and 1964 tsunami was investigated in more detail by GILMOUR (1990), who noted an additional spectral peak at 214 min for the 1960 event that was not observed in Heath's 1976 analysis. It is worth noting that the 96 min peak noted by HEATH (1976) is not
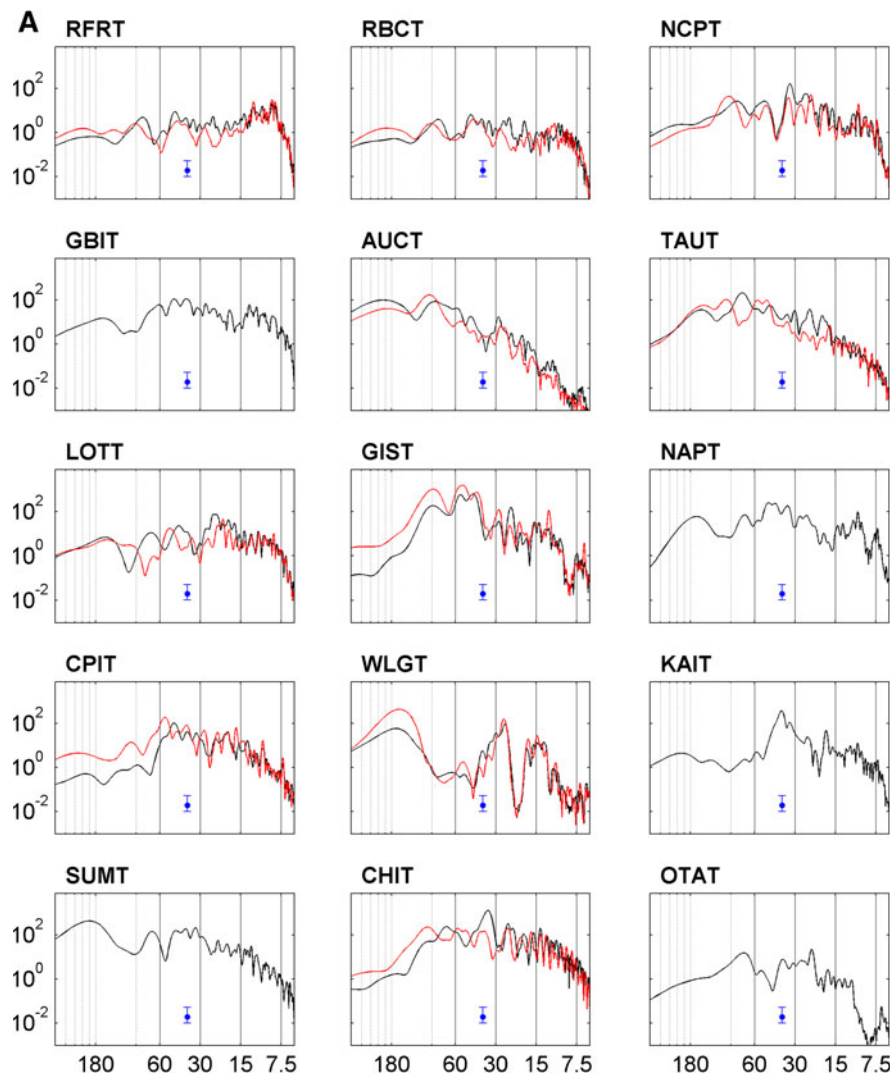
Figure 6

FFT analysis for the tide gauges comparing the Chile tsunami (*red*) with the Japan tsunami (*black*) at: **a** GNS New Zealand, **b** NIWA New Zealand, and **c** NOAA California. *Horizontal axis* is wave period in minutes, and *vertical axis* is energy density in cm^2/cph

present in those results, but rather lower-frequency peaks are evident for both tsunamis between 101 and 138 min. Both HEATH (1976) and GILMOUR (1990) identify enhanced spectral energy at periods of ∼30 and ∼17 min. These correspond well with the higher resonant modes identified for Wellington Harbor by ABRAHAM (1997).

GORING (2002) analyzed the response of several New Zealand tide gauges to the 23 June 2001 Peru tsunami, applying the technique of wavelet analysis to the tsunami records. His analysis decomposed the water level signal recorded at Lyttelton and nearby

Sumner Head into several frequency bands illustrating the wave activity in each. He noted that the tsunami energy amplified ultralong waves that were present prior to tsunami arrival. This effect was also observed in the water level record at Lyttelton from the 2011 Tohoku tsunami and is reported in GORING (2011) and BORRERO *et al.* (2012). More recently, TOLKOVA and POWER (2011) used synthetic tsunami signals to quantify the natural oscillatory modes of Monterey Bay in California and Poverty Bay (Gisborne) in New Zealand. Additionally, an excellent resource describing the background spectra and
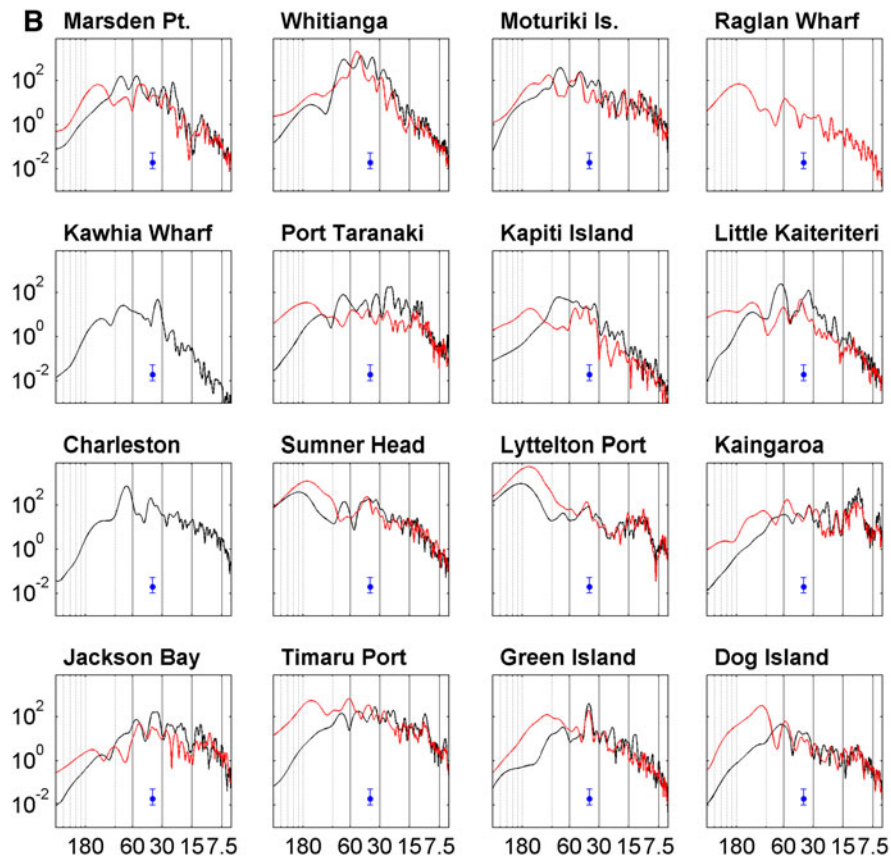
Figure 6
continued

resonant characteristics of several New Zealand tide gauge sites is presented online at: http://www.tideman.co.nz/GeoNet/LWSpectra.html (Accessed 31 July 2012) (GORING, unpublished report).

4.2.2 FFT: 2011 Japan Compared with 2010 Chile in New Zealand

While some sites show a strong similarity in the spectral signature between the two events, there are also some striking differences. For example, WLGT, GIST, Sumner Head, and Lyttelton each have similar spectral signatures for both tsunamis; however, Whitianga, Moturiki, and TAUT show some distinct differences. Whitianga, for example, features one strong peak at 51 min during the 2010 Chile tsunami, yet three distinct peaks (36, 47, and 69 min) are evident during the Japan event. On the Moturiki gauge, the two events both show a strong peak at

$\sim$47 min with another strong peak at a lower frequency: approximately 77 min from Japan and 98 min from Chile. The Wellington results are very similar for both events with peaks at 156–168, 26, and 12–17 min. These values compare well with the periods of the first, third, and sixth resonant modes of Wellington Harbor as described by ABRAHAM (1997).

It is interesting to note the difference in the spectral character of the tide gauge response in the Chatham Islands where two stations, CHIT and Kaingaroa, recorded both events. The CHIT station shows several coincident peaks at periods shorter than 30 min; however the peak at 36 min during the Japan event dominates the record. At longer periods, the Japan event shows a peak at $\sim$70 min while the Chile tsunami has a peak at 99 min. The Kaingaroa gauge on the other hand is quite different, with energy from both the Chile and Japan tsunamis concentrated in the higher frequencies. Only the
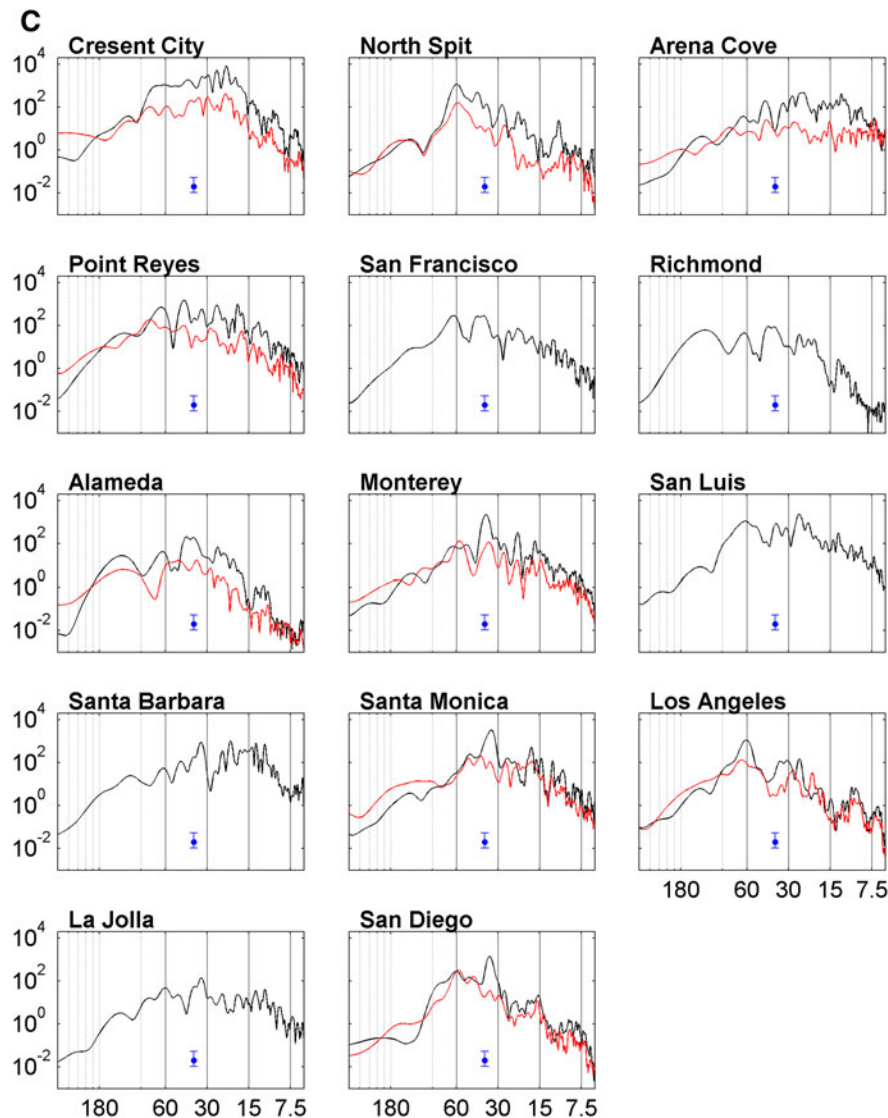
Figure 6
continued

4.2.3 FFT: 2011 Japan Compared with 2010 Chile in California

Chilean event shows appreciable low-frequency energy with a peak at 56 min.

On the three stations in the Christchurch area (SUMT, Lyttelton, and Sumner Head), the resonance of the 204-min-period Pegasus Bay seiche (GORING and HENRY 1998) is evident on all three stations during the Japan event, indicated by the spectral peak at 195–208 min. The Chile tsunami however resonated at a slightly shorter periods of 152 and 164 min at Lyttelton and Sumner Head, respectively. This is discussed in more detail in Sect. 4.3.1.

Inspection of the FFT results from the California stations (Fig. 6c) shows that the response to the Japan tsunami was generally much greater than for the Chilean tsunami, particularly on gauges north of Point Conception. On the southern stations (San Diego, La Jolla, Los Angeles, and Santa Monica), the two signals are comparable in terms of energy, however the Japan event shows a strong peak

Table 4

Wave periods (in minutes) associated with the four strongest spectral peaks derived from FFT analysis of the Chile and Japan tsunamis on the (a) GNS gauges in New Zealand, (b) NIWA gauges in New Zealand, (c) NOAA gauges in California, and (d) DART tsunameters

Station	GNS–Chile Peak period (min)				Station	GNS–Japan Peak period (min)			
	1	2	3	4		1	2	3	4
A									
RFRT	9–12	44	90	27	RFRT	8–12	45	80	
RBCT	39–44	11	91	28	RBCT	46	38	81	24–26
NCPT	23	93	34	10	NCPT	33	23–25	51	81
GBIT	N/A	N/A	N/A	N/A	GBIT	38–47	27	13	60
AUCT	93	190	28		AUCT	208	86	46	29
TAUT	97	49–57	141		TAUT	74	46	23	148
LOTT	18–22	51			LOTT	16–23	43	69	152
GIST	42–53	87	29	12	GIST	44	55	89	23
NAPT	N/A	N/A	N/A	N/A	NAPT	34–47	10	71	161
CPIT	55	38	16	28	CPIT	47	38	19	32
WLGT	156	26	12–17		WLGT	26	168	13–17	
KAIT	N/A	N/A	N/A	N/A	KAIT	38	18		
SUMT	N/A	N/A	N/A	N/A	SUMT	199	32–46	69	
CHIT	97	24	51–57	37	CHIT	34	24	70	
OTAT	N/A	N/A	N/A	N/A	OTAT	23	72	37	

Station	NIWA–Chile Peak period (min)				Station	NIWA–Japan Peak period (min)			
	1	2	3	4		1	2	3	4
B									
Marsden Pt.	44–51	132	28		Marsden Pt.	55	79	23	29
Whitianga	51	35	29		Whitianga	47	36	69	27
Moturiki Is.	48	98	16	11	Moturiki Is.	74	47	30–36	
Raglan Wharf	171	58			Raglan Wharf	N/A	N/A	N/A	N/A
Kawhia Wharf	N/A	N/A	N/A	N/A	Kawhia Wharf	33	74	124	
Port Taranaki	164	40	57	13	Port Taranaki	23–25	74	42	
Kapiti Island	41	53	25	146	Kapiti Island	34–76	25		
Little Kaiteriteri	40	124	60		Little Kaiteriteri	64	34	124	18
Charleston	N/A	N/A	N/A	N/A	Charleston	69	39	21	
Sumner Head	164	41	33		Sumner Head	195	33–46	69	
Lyttelton Port	152	40	11		Lyttelton Port	186	39	69	
Kaingaroa	55	29–33	11–12	17	Kaingaroa	10–13	21	32	
Jackson Bay	51	35–38	27	21	Jackson Bay	34–37	55		
Timaru Port	61	146	39	27	Timaru Port	34	22–25	49	10
Green Island	38	102			Green Island	38	69	22	13
Dog Island	100	58	35–40		Dog Island	63	36–42	11	

Station	CA–Chile Peak period (min)				Station	CA–Japan Peak period (min)			
	1	2	3	4		1	2	3	4
C									
Crescent City	22	30	35		Crescent City	22	26	29–33	41
North Spit	59	27			North Spit	59	43	28	21
Arena Cove	43	7–8	15		Arena Cove	24–28	12	44	
Point Reyes	77	45	60	17	Point Reyes	44	18	26	63
San Fransisco	N/A	N/A	N/A	N/A	San Fransisco	63	38–42	22	
Richmond	N/A	N/A	N/A	N/A	Richmond	38–42	120	63	25

Table 4 *continued*

Station	CA–Chile Peak period (min)				Station	CA–Japan Peak period (min)			
	1	2	3	4		1	2	3	4
Alameda	36	48–55	28	120	Alameda	38–42	25	63	123
Monterey	57	35	27	17	Monterey	37	22	31	50–64
San Luis	N/A	N/A	N/A	N/A	San Luis	22–25	32–37	61	13
Santa Barbara	N/A	N/A	N/A	N/A	Santa Barbara	20	33	13	12
Santa Monica	40	49	17	26	Santa Monica	34	17	22–25	14
Los Angeles	65	28	20	10	Los Angeles	60	31–34	25	10
La Jolla	N/A	N/A	N/A	N/A	La Jolla	33	60		
San Diego	59	45	30–34	15	San Diego	35	60	15	

Station	DART–Chile Peak period (min)				Station	DART–Japan Peak period (min)			
	1	2	3	4		1	2	3	4
D									
21418	N/A	N/A	N/A	N/A	21418	45	71		
21413	114	50	35	17	21413	73	47	33	19
52403	37				52403	73	41	21	25
51407	N/A	N/A	N/A	N/A	51407	45	76		
46412	46	17	20	28	46412	35	85	25	47
51425	38	28	59	7	51425	79	47	23	35
43412	N/A	N/A	N/A	N/A	43412	36	22	71	25
51406	114	50	27–31		51406	82	33	47	14–19
32412	N/A	N/A	N/A	N/A	32412	44	32	21	13
32401	N/A	N/A	N/A	N/A	32401	44	76	32	25

between 30 and 40 min on several gauges including San Diego, Santa Monica, Santa Barbara, and Monterey. This peak is also evident, but less pronounced, on several other stations including La Jolla, Los Angeles, San Luis, and Point Reyes. We also note that our computed spectral peak of 33–34 min for Santa Monica and La Jolla roughly matches the peak at 37.5 min presented by RAICHLEN (1970) for these two stations during the 1964 Alaska tsunami. There is a difference however in the dominant frequency for Los Angeles; our analysis puts it at 60 and 65 min during the Japan and Chile events, while in the RAICHLEN (1970) study, the peak sits at a much shorter 33.3 min for both the 1960 and 1964 tsunamis with strong secondary peaks evident at 150 min in 1960 and 100 min in 1964.

In San Francisco Bay, the San Francisco, Alameda, and Richmond stations all show a similar response to the Japan tsunami with a strong peak at ∼40 min with an additional peak at 61–62 min. On the San Francisco station the 63 min peak is strongest, while at Richmond and Alameda it is the third strongest. Additionally, Richmond and Alameda show a broad hump in the spectrum at 114–116 min. Only the Alameda station has data for comparison with the Chile tsunami. This comparison indicates that the Chilean event was much less energetic in San Francisco Bay, a notion that is confirmed on the Point Reyes gauge, which sits on the open coast just north of the Bay entrance.

4.3. Discussion of Wavelet Spectrograms

Wavelet analysis follows the evolution of the frequency content of the sea level record over the duration of the tsunami event. A wavelet spectrogram plot is a vivid means of visualizing the changes in spectral content of a signal over time. In Figs. 7, 8, 9, 10 we compare spectrograms at sites of interest for the Chilean and Japan tsunamis in New Zealand and California. Table 5a–d presents the timing and period

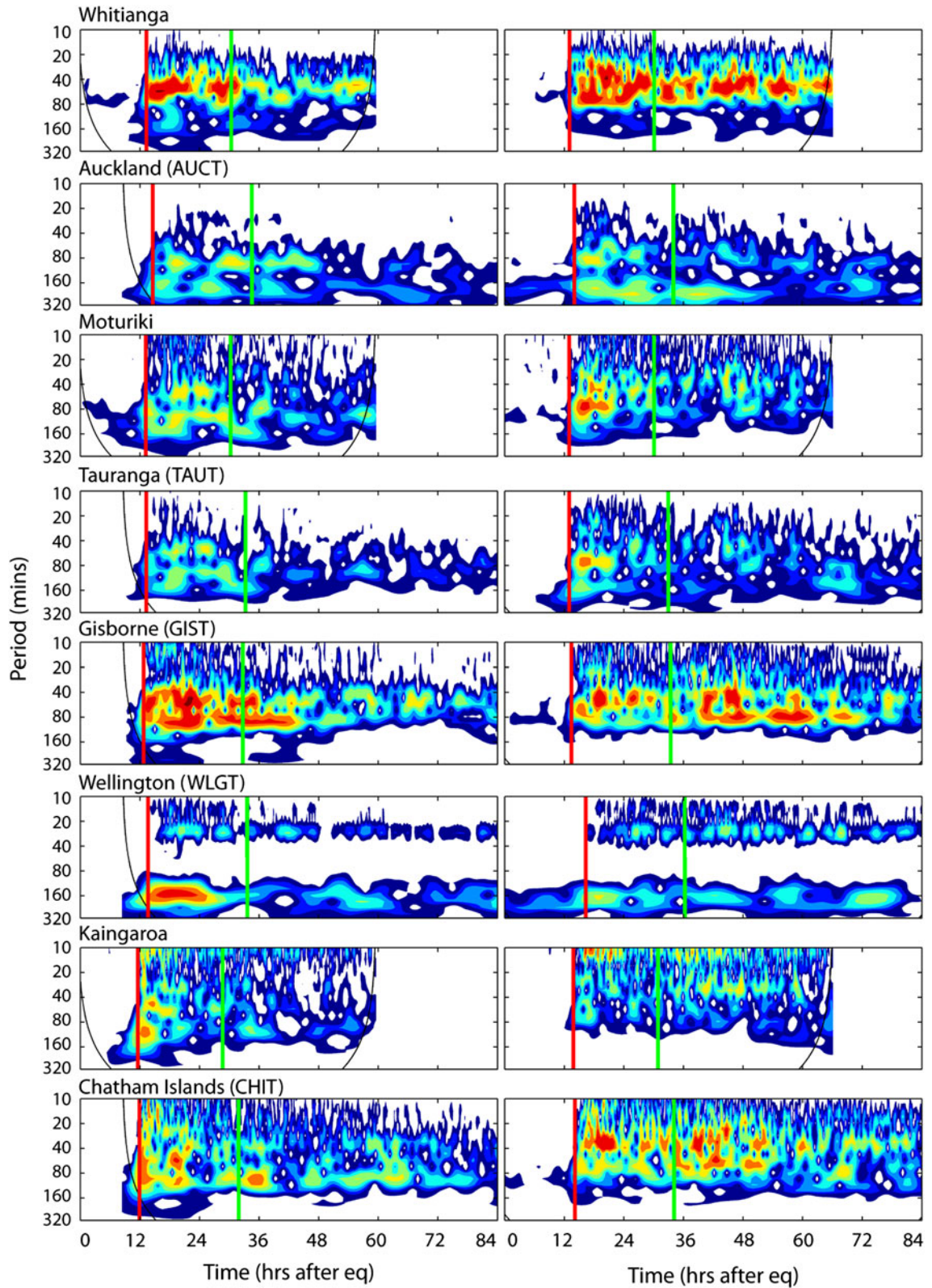◄   Figure 7
Wavelet spectrograms at select sites in New Zealand comparing the
Chile tsunami (*left column*) with the Japan tsunami (*right column*).
Vertical axis is wave period in minutes, and *horizontal axis* is hours
after the causative earthquake. *Colors* represent signal strength.
Vertical red lines indicate the tsunami arrival, and *vertical green
lines* denote the end of the data segment used in the FFT analysis

of the maximum power for each spectrogram. The
wavelet analysis is plotted over 3.5 days (84 h) of
data for the GNS and NOAA data and 2.5 days (60 h)
for the NIWA data to illustrate the evolution of the
tsunami signal. A complete set of spectrograms with
the associated water level time series is included as
supplemental figures.

4.3.1 New Zealand Spectrograms

Starting with New Zealand (Figs. 7, 8 and Supple-
mental Figures), we note that Whitianga responded
more energetically to the Japan tsunami. There was
also a broader spread of wave periods showing
significant power. This is reflected in the three peaks
noted in the FFT analysis above. While the Chilean
tsunami tapered significantly 24 h after arrival,
energy from the Japan event persisted at consistent
levels for at least another 36 h. At AUCT, the
Chilean event was slightly more energetic and longer
lasting than Japan. Also, the energy from the Chile
event peaked much later in the time series, some 16 h
after arrival, whereas it occurred 3.2 h after arrival
during the Japan event. It is also interesting to note
the difference between the Moturiki signal and
TAUT, which shows a weaker overall response than
Moturiki. This is expected since Moturiki sits on the
open coast while TAUT is inside Tauranga Harbor.
The two stations have similar characteristics in terms
of frequency range and timing for each event,
however the Chilean tsunami shows a bimodal
frequency distribution with peaks at ∼50 min and
∼98 min while the Japan tsunami just shows one
strong spectral peak at ∼74 min.

On the east coast, Gisborne (GIST) responded
more strongly to the Chilean tsunami, however the
overall duration was not as long as during the Japan
event. For both events, the GIST signals shows
spectral peaks and substantial energy at periods of
approximately 60 and 90 min, periods identified by
Tolkova and Power (2011) as the shelf resonance

modes for Poverty Bay (where Gisborne is located).
Upon arrival, the Chile tsunami signal contained the
bulk of the energy in the 60 min band, which rapidly
shifted to the 90 min band, before settling into a
bimodal phase with energy at both periods that slowly
tapered over the next 36–48 h. This is in contrast to
the Japan tsunami, which first arrived with energy at
∼70 min, then shifted to 60 min, where it remained
dominant for the next 24 h. A resurgence in energy
from the Japan tsunami begins some 40 h after the
earthquake. This resurgence is bimodal at ∼60 and
90 min, and we interpret this part of the signal to be a
reflection of the tsunami off of South America as its
spectral signature is similar to that for the Chile
tsunami, which would have arrived from the same
direction as the reflected waves, and because the
arrival time matches that for a long wave traveling
from Japan to South America and back to New
Zealand. We also note that early on in the Japan
tsunami, appreciable energy is seen in the higher
frequency (∼25 min) band that is not evident in the
Chilean tsunami. This resonance period corresponds
to the second normal mode of Poverty Bay, identified
by Tolkova and Power (2011). Perhaps the oblique
approach direction of the Japan tsunami was a factor
in the lower level of initial excitation of the shelf
waves and allowing for the Poverty Bay seiche to be
evident.

At Wellington, a distinctly trimodal spectral
signature is apparent during both events, with the
Chilean tsunami creating a stronger overall response.
Finally, the Chatham Island stations of Kaingaroa and
CHIT are noted for their differences, despite being
located very close to each other on opposites sides of
a small island. In the Chilean tsunami, Kaingaroa
experienced a stronger signal than from Japan, with
more energy affecting the station early in the event
and at a lower frequency, whereas during the Japan
tsunami more high-frequency energy was present and
this signal lasted longer. At CHIT, the results are
similar in terms of duration, but there is more low-
frequency energy persisting for much longer during
the Japan event.

The stations on the east coast of the South Island
(Sumner Head, Lyttelton Port, SUMT, and Timaru)
are presented separately in Fig. 8. These stations are
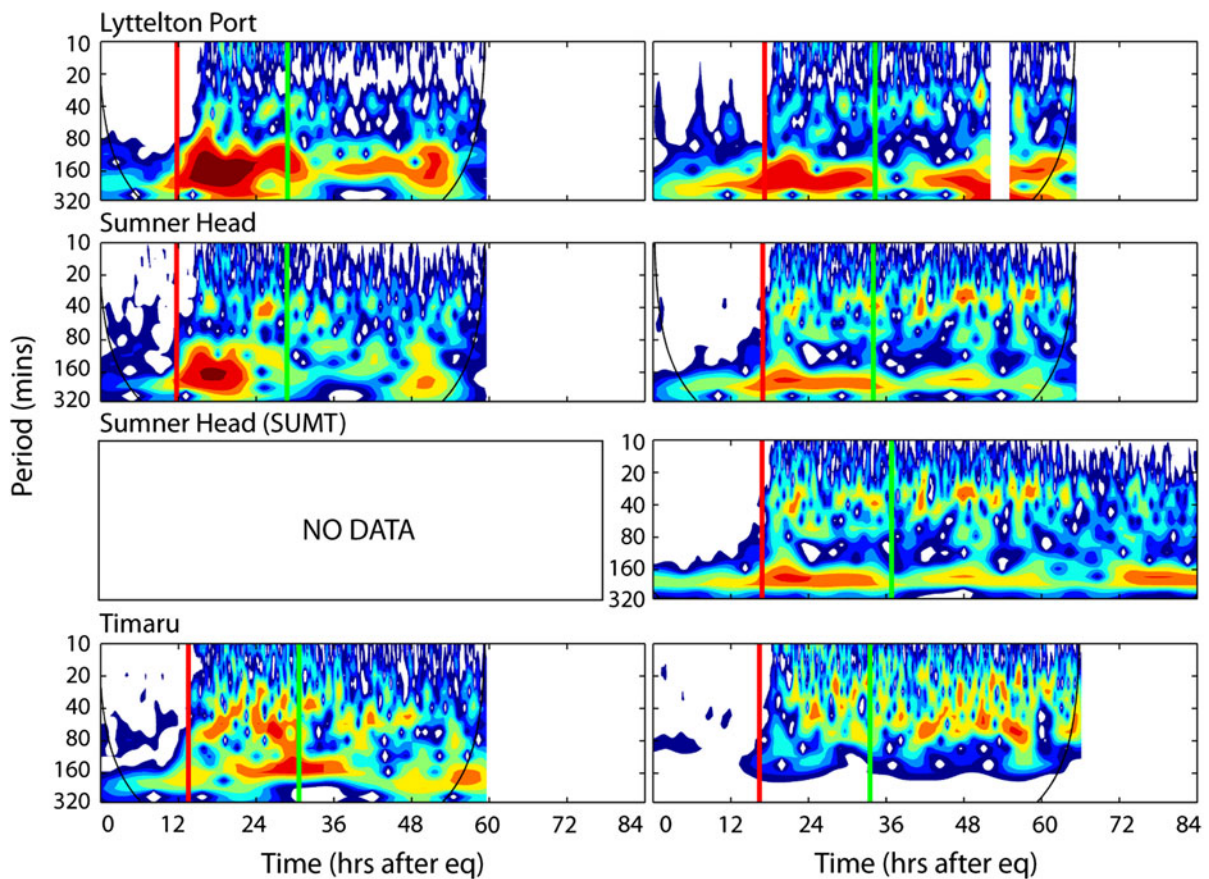important in that they show the effects at two

Figure 8
Wavelet spectrograms at sites on the east coast of the South Island of New Zealand for the Chile tsunami (*left column*) and the Japan tsunami (*right column*). *Vertical axis* is wave period in minutes, and *horizontal axis* is hours after the causative earthquake. *Colors* represent signal strength. *Vertical red lines* indicate the tsunami arrival, and *vertical green lines* denote the end of the data segment used in the FFT analysis

important New Zealand ports (Lyttelton and Timaru) and clearly show long-wave seiching. On the Sumner Head, Lyttelton Port, and SUMT stations, the Pegasus Bay seiche, which resonates at ~204 min (GORING and HENRY, 1998), was amplified during the Japan tsunami. The spectrograms show that this seiche was active prior to tsunami arrival and was then amplified, as first noted by GORING (2011) and described in BORRERO *et al.* (2012). Also evident in the spectrograms for Lyttelton is the second mode of the Lyttelton Harbor seiche, known to resonate at approximately 40 min (DEREK GORING, pers. comm.). As noted in the FFT discussion above, during the Chile tsunami, the low-frequency resonance occurred at a slightly shorter period than during the Japan tsunami. Inspection of the Lyttelton and Sumner

Head spectrograms (Fig. 8) shows that the initial burst of tsunami energy from Chile contained the bulk of its energy at periods between approximately 150 and 170 min with a peak at 157 min occurring approximately 9 h after tsunami arrival (Table 5b). The spectrograms do suggest the activation of the longer (~204 min) Pegasus Bay seiche, but it is not as pronounced or long lasting as during the Japan tsunami. It is important to note the strong response at

Figure 9   ▶
Wavelet spectrograms at sites in California comparing the Chile tsunami (*left column*) with the Japan tsunami (*right column*). *Vertical axis* is wave period in minutes, and *horizontal axis* is hours after the causative earthquake. *Colors* represent signal strength. *Vertical red lines* indicate the tsunami arrival, and *vertical green lines* denote the end of the data segment used in the FFT analysis
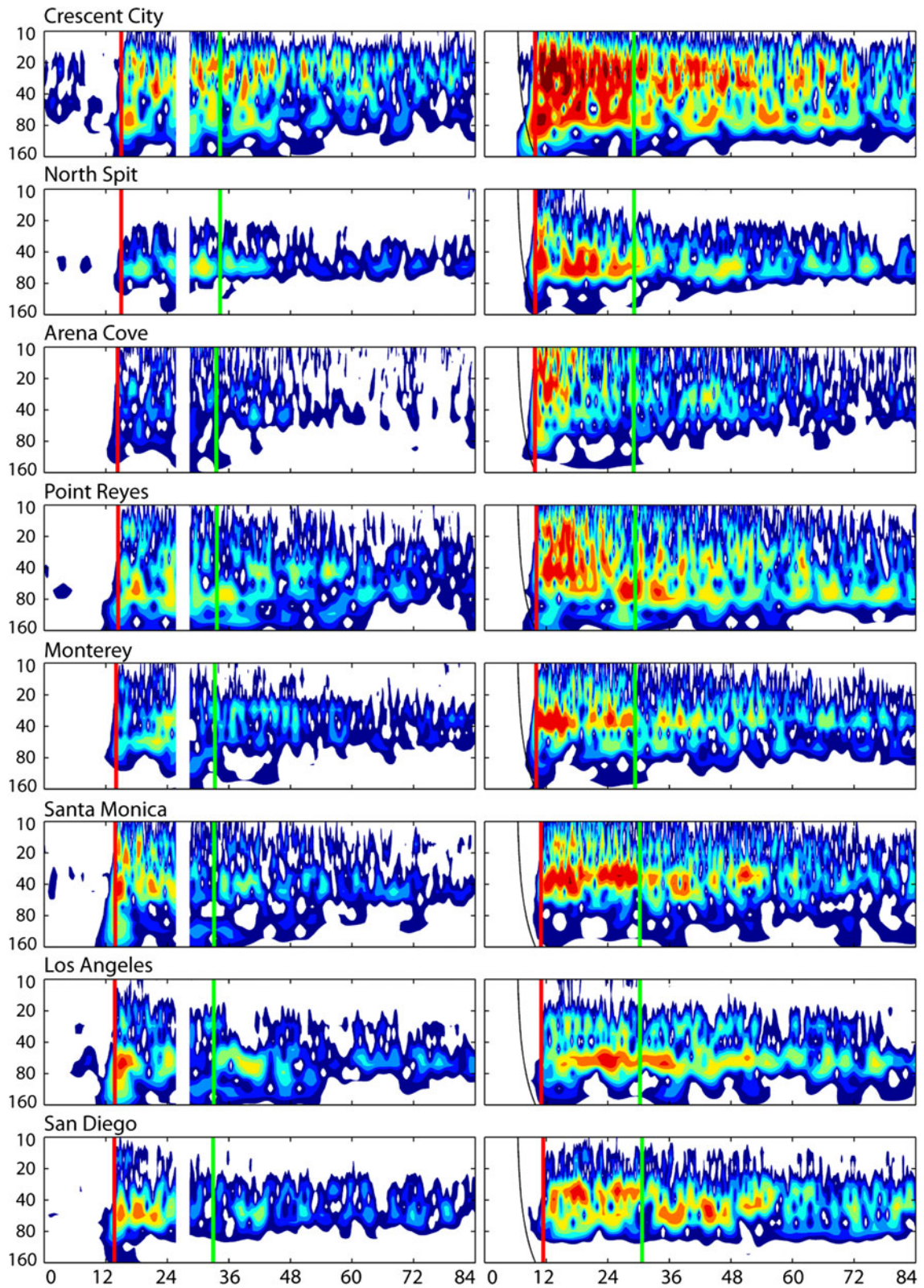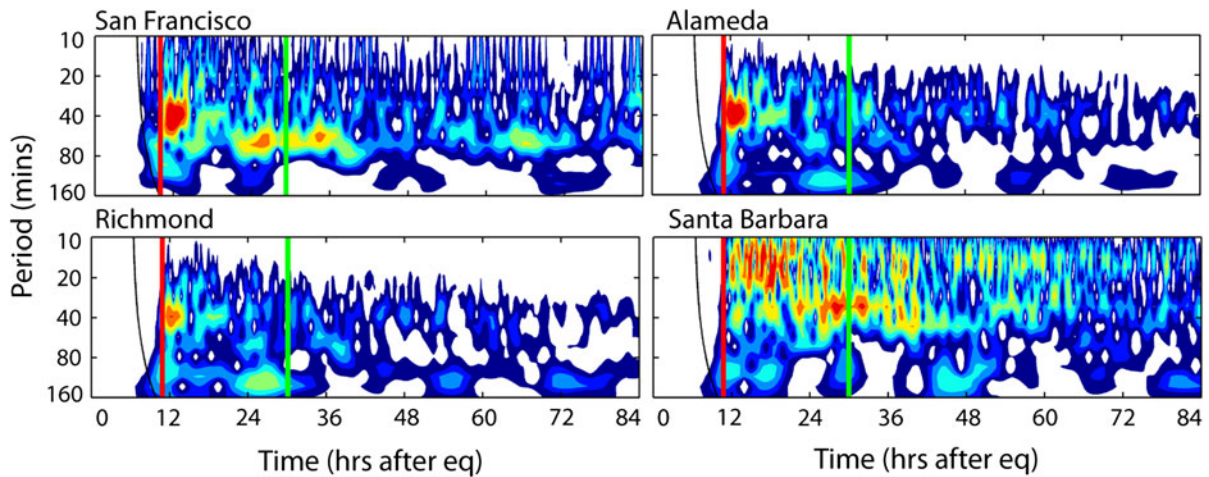
Figure 10
Wavelet spectrograms at sites in California during the 2011 Japan tsunami. *Vertical axis* is wave period in minutes, and *horizontal axis* is hours after the causative earthquake. *Colors* represent signal strength. *Vertical red lines* indicate the tsunami arrival, and *vertical green lines* denote the end of the data segment used in the FFT analysis

the Lyttelton station during the Chilean tsunami as compared with Japan, clearly indicating the vulnerability of the port to tsunamis originating from South America.

The Timaru record of the Chile tsunami shows the late occurrence of the strongest signal, with peak wave energy arriving some 18 h after tsunami arrival at periods of 132–146 min (Tables 4b, 5b). These values compare well with the 146 min period of the Canterbury Bight seiche identified by GORING and HENRY (1998). Interestingly, this edge wave mode was not amplified during the Japan tsunami and peak energy was concentrated in higher frequencies with spectral peaks at 34, ∼24, and 49 min, and maximum power at a period of 66 min occurring 40 h after tsunami arrival. We hypothesize that the wave approach direction of the Japan tsunami prevented it from activating the Canterbury Bight seiche as wave energy was trapped and focused to the north and east by the Chatham Rise, a bathymetric ridge extending eastward from central New Zealand to the Chatham Islands with depths of <500 m. We also note that reflected energy during the Japan tsunami did not excite the Canterbury Bight seiche as there is no appreciable energy at a period of 144 min seen in the data. In addition to these sites, the Chilean tsunami was more energetic at other east coast stations (i.e., CPIT, Green Island, and Dog Island), highlighting the

vulnerability of this area to tsunamis originating in South America.

4.3.2 California Spectrograms

Moving to the California stations, the wavelet spectrograms also illustrate the extended duration of both the Chile and Japan tsunamis (Figs. 9, 10 and Supplemental Figures). It is clear that the Japan tsunami was much more energetic, particularly at stations north of Point Conception. The Chilean tsunami, however, did have significant effects at opposite ends of California—in the far north at Crescent City, a known amplifier for long-wave energy (GONZÁLEZ *et al.*, 1995; KOWALIK *et al.*, 2008; HORILLO *et al.*, 2008), and in southern California. The strength and duration of the Japan tsunami on the southern California stations are also notable, with the Santa Monica, Los Angeles, and San Diego stations showing a strong signal out to 60 h. The evolution of the tsunami signal at Monterey follows a similar pattern to that seen in Gisborne (GIST). The tsunami with the more oblique approach angle (the Chilean tsunami for Monterey, Japan for Gisborne) energizing a lower frequency first, which then transitions to a higher-frequency mode. For the tsunami with the more direct approach azimuth (Japan in CA and Chile in NZ), the higher-frequency modes are activated first with the lower frequencies

Table 5

Timing of the maximum power and associated wave period for the (a) GNS gauges in New Zealand, (b) NIWA gauges in New Zealand, (c) NOAA gauges in California, and (d) DART tsunameters

Station	Chile		Japan	
	Time (h)	Period (min)	Time (h)	Period (min)
GNS (**A**)				
RFRT	1.2	8	1.8	33
RBCT	4.7	39	1.7	33
NCPT	5.9	23	9.3	33
GBIT	N/A	N/A	3.3	39
AUCT	16.2	93	3.2	79
TAUT	5.9	56	3.2	66
LOTT	1.1	20	7.9	20
GIST	8.9	56	5.7	47
NAPT	N/A	N/A	35.5	39
CPIT	1.9	57	30.5	47
WLGT	5.1	157	51.4	28
KAIT	N/A	N/A	47.2	33
SUMT	N/A	N/A	4.0	187
CHIT	7.4	57	5.9	33
OTAT	32.5	222	37.9	79
NIWA (**B**)				
Marsden Pt.	10.5	47	7.0	66
Whitianga	2.6	56	7.4	39
Moturiki Is.	10.9	47	3.1	79
Raglan Wharf	11.7	157	N/A	N/A
Kawhia Wharf	N/A	N/A	12.5	66
Port Taranaki	12.5	157	9.1	23
Kapiti Island	22.2	56	17.2	66
Little Kaiteriteri	15.7	39	20.1	66
Charleston	N/A	N/A	7.5	66
Sumner Head	5.6	157	3.7	187
Lyttelton Port	6.6	157	3.7	187
Kaingaroa	1.5	111	3.6	10
Jackson Bay	8.0	33	4.5	33
Timaru Port	16.4	132	39.7	66
Green Island	2.5	94	9.7	39
Dog Island	10.5	111	7.0	79
US (**C**)				
Crescent City	6.8	33	2.58	28
North Spit	15.88	56	1.12	47
Arena Cove	2.89	23	2.53	28
Point Reyes	3.5	66	2.3	39
San Francisco	N/A	N/A	1.94	39
Richmond	N/A	N/A	1.41	39
Alameda	4.55	47	1.54	39
Monterey	9.99	39	3.93	33
San Luis	N/A	N/A	1.46	23
Santa Barbara	N/A	N/A	7.47	20
Santa Monica	0.65	47	15.22	33
Los Angeles	1.41	66	12.66	56
La Jolla	N/A	N/A	13.01	33
San Diego	4.62	56	6.46	33

Table 5 *continued*

Station	Chile		Japan	
	Time (h)	Period (min)	Time (h)	Period (min)
DART (**D**)				
21418				
21413	22.4	111	1.5	33
52403	22.5	39	8.2	66
51407	N/A	N/A	9.3	79
46412	13.3	17	13.3	79
51425	16.4	28	8.8	23
43412	N/A	N/A	13.8	17
51406	9.0	39	15.1	79
32412	N/A	N/A	22.2	33
32401	N/A	N/A	25.1	79

Times are in hours after tsunami arrival for the coastal tide gauges and hours after the earthquake for the tsunameters

responding somewhat later. In general, the results of our analysis follow the observations of MILLER *et al.* (1962) regarding the decay of the tsunami signal in that the overall shape of spectrum remains constant as the signal fades and that higher frequencies decay faster than lower frequencies.

On stations located in San Francisco Bay (Fig. 9), from the Japan tsunami we see a packet of wave energy at ~40 min period affecting the San Francisco, Alameda, and Richmond gauges at the beginning of the data record. That burst of energy dissipates rapidly and transitions to longer periods of ~60 min on the San Francisco gauge and 120 min on Alameda and Richmond. On the Santa Barbara record (Fig. 9) we see that the signal is rich in higher-frequency energy, more so than in any of the other southern California gauges. We interpret these 10–20 min oscillations to be the scattering and reflecting of the tsunami waves off of the Channel Islands that sit to the south of Santa Barbara (Fig. 2). Indeed, we see some similar higher-frequency energy on the Santa Monica station, which is positioned such that it too would intercept the scattered tsunami wave energy that had passed through the Channel Islands.

5. DART Tsunameter Data

We selected a subset of the available DART tsunameter data for analysis. The stations used in this

study are indicated in Fig. 11, accompanied by the wavelet spectrogram from the Japan tsunami at each site. Presented in this manner, we can visualize the evolution of the tsunami signal as it spreads across the Pacific. The frequency signature of the initial pulse crossing station 21418 is very broad with a strong peak evident at 45 min. By the time the tsunami has reached the next station (21413) the energetic frequencies become more discrete with peaks at 47, 33, and 66 min. It is interesting to note the similarity of the FFT for station 21413 (Fig. 12) to the FFT of the data recorded at Whitianga in northern New Zealand (Fig. 6b) as both exhibit three spectral peaks at nearly the same frequencies (compare in Table 4b, d). Inspection of the NOAA modeling results for the Japan tsunami (Fig. 1, lower

left inset) shows a strong beam of energy emanating from the source region and extending directly into the northern New Zealand Bight. That this path runs virtually unobstructed from the source region to northern New Zealand, passing just east of Vanuatu and west of Fiji, may explain the similarity between these two records.

As the tsunami signal radiates outward, we note that station 52403 (nearly due south) does not show the distinct peaks still evident on 51407 (Hawaii) and 46412 (southern California) but rather shows a broad hump centered on 71 min. Indeed a low-frequency peak between 76 and 85 min is seen on all of the DART stations (Table 4d). While the signal is somewhat attenuated on stations 51425 (near Fiji) and 43412 (west of Mexico), station 51406 in the central eastern
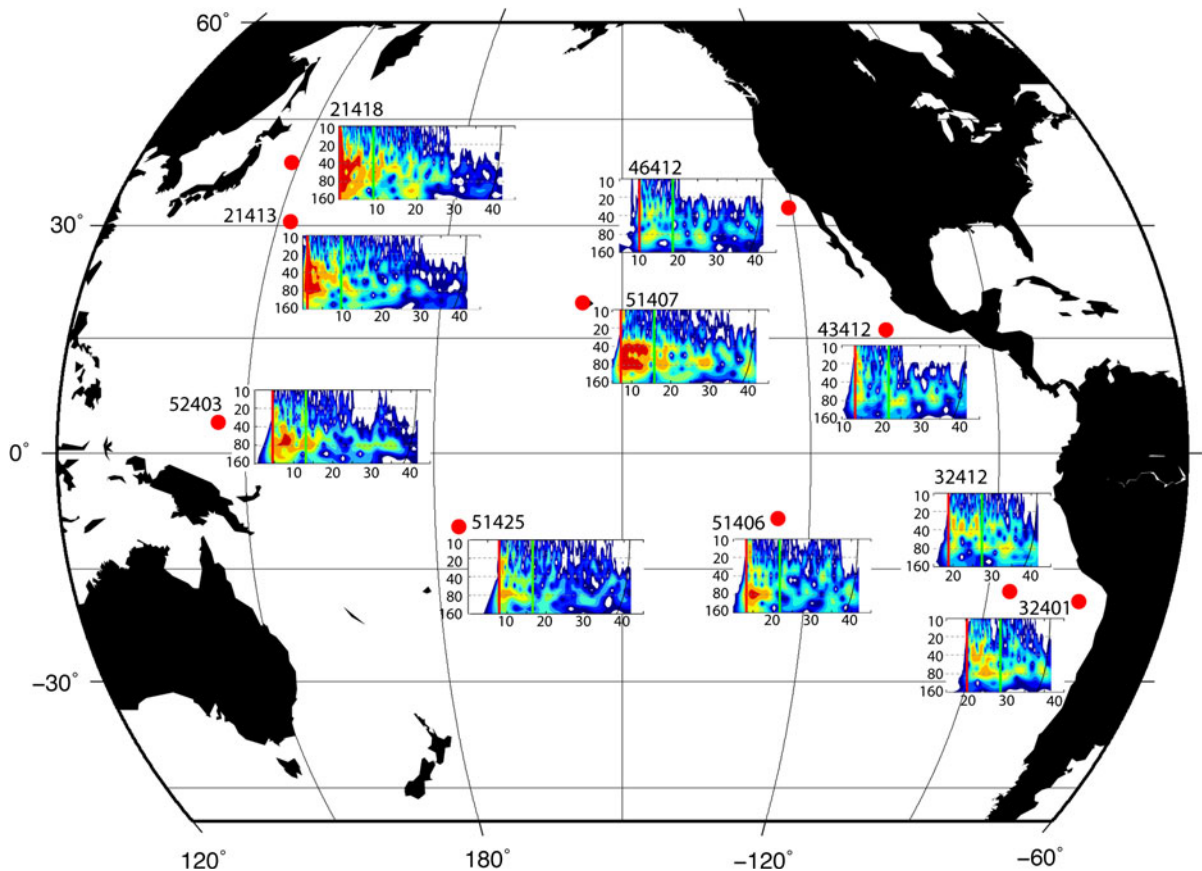

Figure 11

Locations of DART tsunameters and accompanying wavelet spectrograms for each showing the evolution of the Japan tsunami as it traversed the Pacific Basin. The *vertical axis* on each spectrogram is wave period in minutes, and the *horizontal axis* is hours after the causative earthquake. *Colors* represent signal strength. *Vertical red lines* indicate the tsunami arrival, and *vertical green lines* denote the end of the data segment used in the FFT analysis
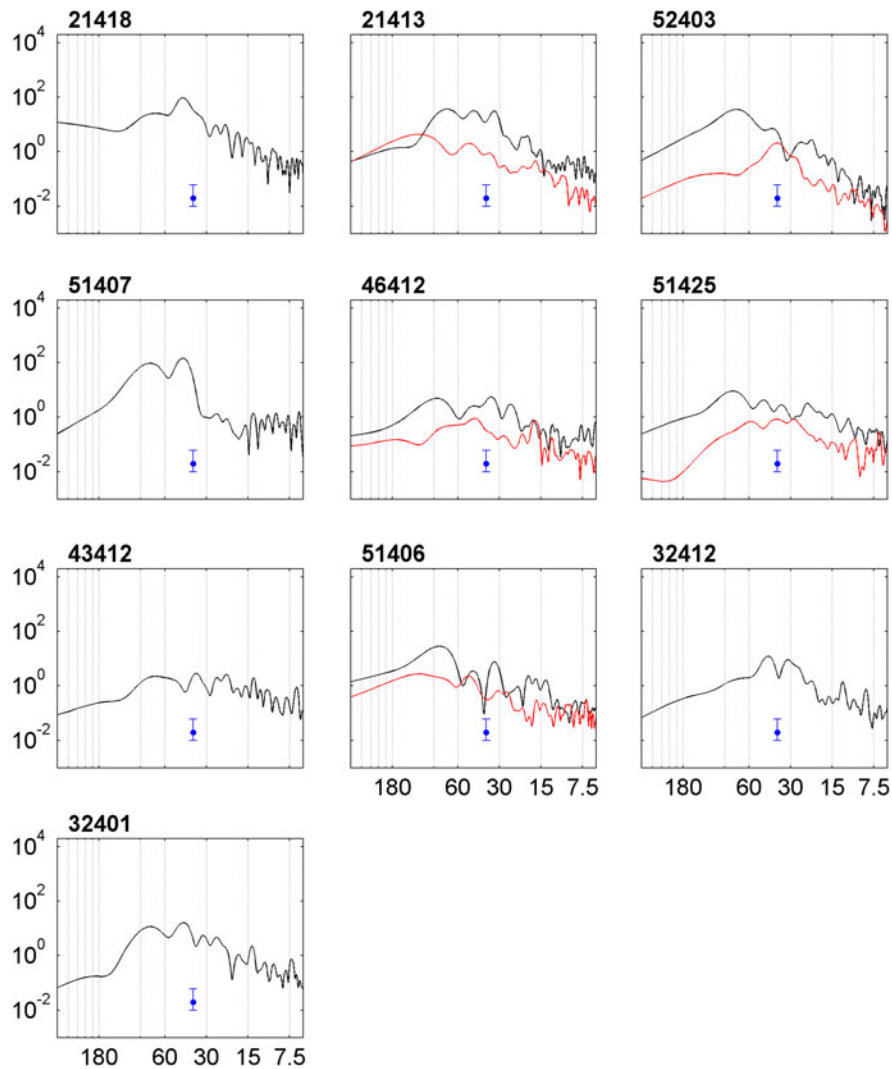
Figure 12
FFT analysis of the DART tsunameter records comparing the Chile tsunami (*red*) with the Japan tsunami (*black*)

South Pacific shows considerable energy. Approaching South America, stations 32412 and 32401 differ in that 32412 does not show the long-period energy that is seen on many of the other gauges.

Only five stations from this set had complementary data for the 2010 Chilean tsunami; these are compared in Fig. 13. At station 51406, the Chilean tsunami has considerable energy at somewhat lower frequencies than during the Japan event. Stations 46412, 51425, and 52403 each show relatively low energy levels during the Chile tsunami, as these stations lie east and west of the main energy beam.

Across the Pacific and near Japan at station 21413, the long-period energy not seen on the other three stations is evident once again.

6. Summary and Conclusions

This study was conducted to present baseline data on the characteristics of far-field tsunamis affecting the coasts of New Zealand and California and to systematically explore the evolution of the spectral signature of a strong tsunami throughout an entire
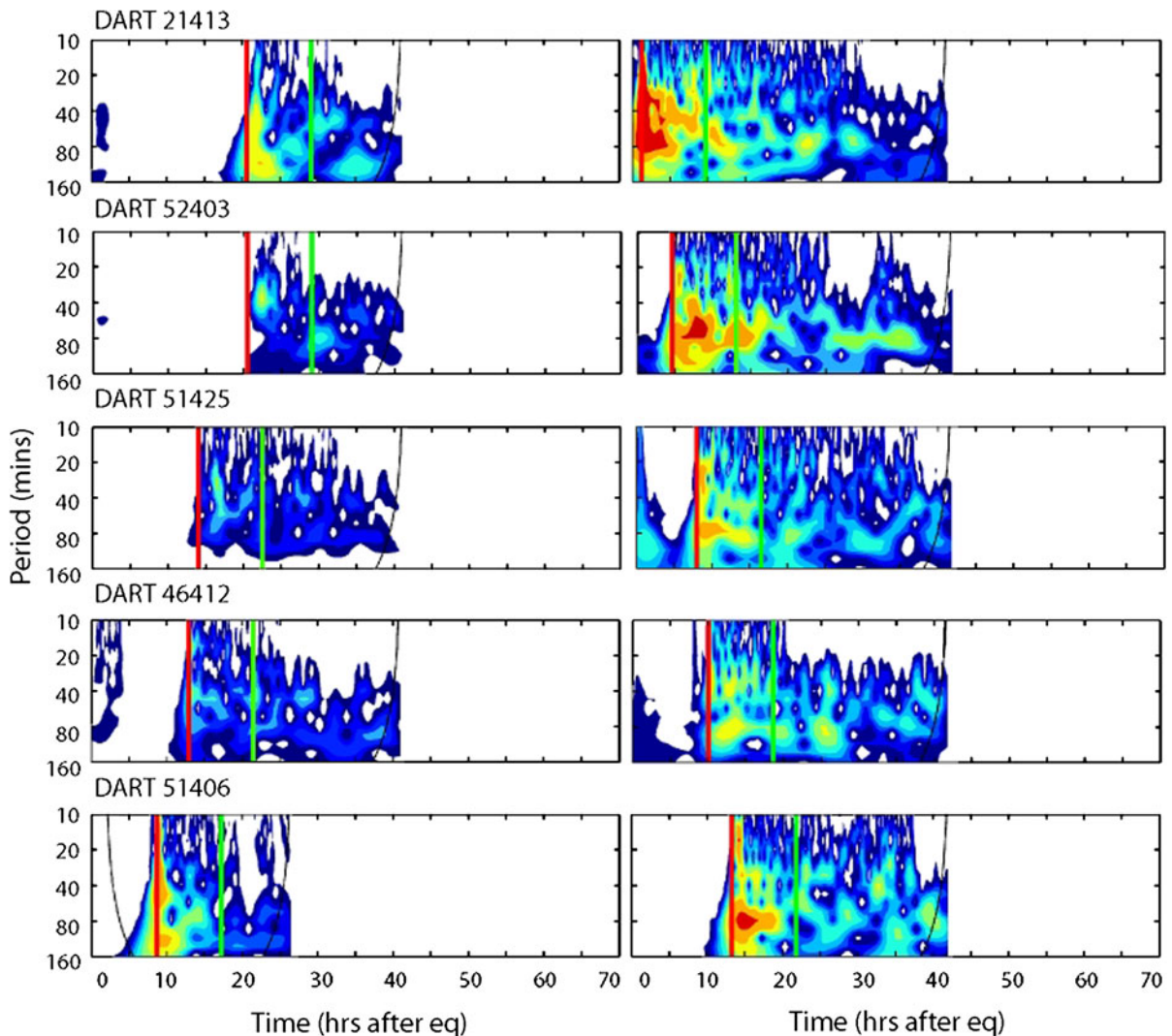
Figure 13
Comparison between wavelet spectrograms at five DART tsunameter sites for the Chile tsunami (*left column*) and the Japan tsunami (*right column*). *Vertical axis* is wave period in minutes, and *horizontal axis* is hours after the causative earthquake. *Colors* represent signal strength. *Vertical red lines* indicate the tsunami arrival, and *vertical green lines* denote the end of the data segment used in the FFT analysis

ocean basin. The Pacific Ocean has not experienced a major basin-wide event since the 1960s, and advances in tsunami detection and recording infrastructure have greatly increased the availability of high-quality data. The occurrence of two large tsunamis just 1 year apart on opposite corners of the Pacific presents an excellent opportunity to describe the basin-wide effects. Tide gauge records in New Zealand and California were chosen for analysis since neither location was in the tsunami source region and both

only experienced far-field effects. Also, in these areas, the tsunami affected a wide range of maritime infrastructure ranging from small boat harbors to major commercial ports located in both natural and manmade basins. Numerous corresponding eyewitness accounts and descriptions of the effects provide additional details regarding the events.

Our interpretation of the results suggests that the locations of New Zealand and California relative to each source region are somewhat analogous; sources

from Chile affect New Zealand as sources from Japan affect California and vice versa. The shore-perpendicular approach direction of the Chile tsunami in New Zealand and the Japan tsunami in California create some basic similarities in the wave behavior. These events create a response featuring a strong initial burst of incident energy that decays relatively uniformly with time. In both New Zealand and California, stations with a more direct path to the source saw their wave maxima earlier than for stations with a more indirect orientation.

Differences can be seen between the tsunami effects in California as a function of the source region. The southern California stations are more strongly affected by the Chilean event as compared with stations north of Point Conception. However, this demarcation was not evident during the Japan tsunami, with all sites in California experiencing significant tsunami effects. We also note that the data from New Zealand appear to have more interstation variability in the characteristics of the tsunami response, while the California stations are more homogeneous. In New Zealand the data clearly show the enhanced response at Whitianga, Gisborne, and Lyttelton/Sumner regardless of the source region, while the same is evident for Crescent City in California. That these sites are important for both recreational and commercial users highlights the need to focus mitigation efforts on these areas.

The data suggest that both reflections and wave trapping play a role in the extended duration of the tsunami signal and the timing of the wave maxima. During the Tohoku tsunami, some stations on the east coast New Zealand stations saw the largest wave heights, or a resurgence in tsunami energy, 30–40 h after tsunami arrival. This is in the time range when waves reflected off of South America and Antarctica would be affecting New Zealand, as inferred from publicly available travel time maps and animations of the global tsunami propagation released since the event (e.g., NOAA animations and analysis). This additional energy likely contributed to the long duration and enhancement of the tsunami signal at these stations seen late in the data record (Figs. 3, 4, 7, and 8), and we believe this was particularly evident on the Gisborne (GIST) gauge as described in Sect. 4.

In California, however, this effect is not seen during the Chilean tsunami, and it is more likely that trapped edge waves played a greater role than direct reflections in the arrival time of the largest waves. We base this assertion on the observation that several stations experienced the largest waves 15–20 h after tsunami arrival, which is too early to have been caused by a reflection coming off the western shore of the Pacific Ocean. We also note that Crescent City and Monterey saw their largest positive amplitudes early in the event (2.7 and 2.0 h after arrival) but the largest peak-to-trough waves occurred at 15.5 and 9.9 h at each site, respectively. GONZÁLEZ et al. (1995) also described the excitation of edge waves as a contributor to the delayed maximum wave heights in Crescent City after the 1992 Cape Mendocino earthquake and tsunami. The direction of approach of the Chilean tsunami to California would be ideal for the excitation of edge waves in central and northern California, as the tsunami wave crests would arrive nearly perpendicular to the coastline north of Point Conception.

This study also highlights the difficulties encountered when making comparisons between datasets from many different sources due to differences in the particular sampling techniques of the gauges and the degree of data processing carried out by the controlling agency before release to the public. Some of this processing is automated, making it difficult to get to the "raw" data. The problem is compounded when trying to compare results between different datasets such as with our intercomparison between two sets of recording from Sumner Head (near Christchurch) on the east coast of the South Island of New Zealand. Here we noted that subtle difference in the processing techniques, many of which are subjective and at the discretion of the individual conducting the analysis, can lead to significant differences in the results and interpretation, and calls for the standardization of techniques for processing and interpreting tsunami data.

REFERENCES

ABRAHAM, E. (1997), *Seiche modes of Wellington Harbour, New Zealand*, N. Z. J. Mar. Fresh. Res., *31*, 191-200.

BORRERO, J., BELL, R., CSATO, C., DELANGE, W., GREER, D., GORING, D., PICKETT, V. and POWER, W. (2012), *Observations, effects and real time assessment of the March 11, 2011 Tohoku-oki Tsunami in New Zealand*, Pure Appl. Geophys., doi:10.1007/s00024-012-0492-6.

DELOUIS, B., NOCQUET, J.-M., and VALLÉE, M. (2010), *Slip distribution of the February 27, 2010 $M_w = 8.8$ Maule earthquake, central Chile, from static and high-rate GPS, InSAR, and broadband teleseismic data*, Geophys. Res. Lett., *37*, L17305, 7 PP., 2010 doi:10.1029/2010GL043899

EMERY, W. J., and THOMSON, R. E., Data analysis methods in physical oceanography, second and revised edition, (Elsevier, New York, 2003).

FRITZ, H., PETROFF, C., CATALÁN, P., CIENFUEGOS, R., WINCKLER, P., KALLIGERIS, N., WEISS, R., BARRIENTOS, S., MENESES, G., VALDERAS-BERMEJO, C., EBELING, C., PAPADOPOULOS, A., CONTRERAS, M., ALMAR, R., DOMINGUEZ, J., and SYNOLAKIS, C. (2011), *Field survey of the 27 February 2010 Chile tsunami*, Pure Appl. Geophys., *168*, 1989-2010.

FUJII, Y., and SATAKE, K. (2012), *Slip distribution and seismic moment of the 2010 and 1960 Chilean earthquakes inferred from tsunami waveforms and coastal geodetic data*, Pure Appl. Geophys., in press.

GILMOUR, A.E. (1990), *Response of Wellington Harbour to the tsunamis of 1960 and 1964,* N. Z. J. Mar. Fresh. Res., *24*:229-231.

GONZÁLEZ, F., SATAKE, K., BOSS, E., and MOFJELD, H. (1995), *Edge wave and non-trapped modes of the 25 April 1992 Cape Mendocino tsunami,* Pure Appl. Geophys., *144*, 409-426.

GORING, D. (2002), *Response of New Zealand waters to the Peru tsunami of 23 June 2001*, N. Z. J. Mar. Fresh. Res., *36*:225-232.

GORING, D. (2011), *Honshu Tsunami 12-March-2011*, Report to the Lyttelton Port Company, 17 pp.

GORING, D. (unpublished), *Long Wave Fourier Spectra at GeoNet Sites*, *unpublished internet URL:* http://www.tideman.co.nz/GeoNet/LWSpectra.html. Accessed 31 July 2012

GORING, D. and HENRY, R., (1998), *Short period (1-4 h), sea level fluctuations on the Canterbury coast, New Zealand*, N. Z. J. Mar. Fresh. Res., *32*, 119-134.

HEATH, R.A. (1976), *The response of several New Zealand harbours to the 1960 Chilean tsunami, in: Tsunami research symposium 1974.* Bull. R. Soc. N. Z. *15*, 71-82.

HORILLO, J., KNIGHT, W., and KOWALIK, Z. (2008), *Kuril Islands tsunami of November 2006: 2. Impact at Crescent City by local enhancement*, J. Geophys. Res., *113*, C01021, doi:10.1029/2007JC004404.

KOWALIK, Z., HORILLO, J., KNIGHT, W., and LOGAN, T. (2008), *Kuril Islands tsunami of November 2006: 1. Impact at Crescent City by distant scattering,* J. Geophys. Res. *113*, C01020, doi:10.1029/2007JC004402.

MILLER, G., MUNK, W., and SNODGRASS, F. (1962), *Long-period waves over California's continental borderland Part 2. Tsunamis*, J. Mar. Res., *20*, 3-30.

MORI, N., TAKAHASHI, T., YASUDA, T., and YANAGISAWA, H. (2011), *Survey of 2011 Tohoku earthquake tsunami inundation and run-up*, Geophys. Res. Lett., *38*, L00G14, doi:10.1029/2011GL049210.

OZAWA, S., NISHIMURA, T., HISASHI S., KOBAYASHI, T., TOBITA, M., and TETSURO IMAKIIRE, T. (2011), *Coseismic and postseismic slip of the 2011 magnitude-9 Tohoku-Oki earthquake*, Nature, *475*, 373–376.

RABINOVICH, A., and THOMSON, R. (2007), *The 26 December 2004 Sumatra Tsunami: Analysis of Tide Gauge Data from the World Ocean Part 1. Indian Ocean and South Africa*, in: Tsunami and Its Hazards in the Indian and Pacific Oceans Pure Appl. Geophys., doi:10.1007/978-3-7643-8364-0_2

RAICHLEN, F. (1970), *Tsunamis, Some Laboratory and Field Observations,* Proc. of the 12th Intl. Conf. on Coast. Eng., 2103 – 2122.

TORRENCE, C., and COMPO, G. (1998), *A Practical Guide to Wavelet Analysis*, Bull. Am. Met. Soc., *79*, 61-78.

TOLKOVA, E., and POWER W. (2011), *Obtaining natural oscillatory modes of bays and harbors* via *Empirical Orthogonal Function analysis of tsunami wave fields*, Ocean Dynam. *61*:731-751, doi:10.1007/s10236-011-0388-5.